Geochimica et Cosmochimica Acta 336 (2022) 372–393

Contents lists available at ScienceDirect

Geochimica et Cosmochimica Acta

journal homepage: www.elsevier.com/locate/gca

Noble gas evolution of the martian atmosphere in the last 4 Gyr recorded by regolith breccia NWA 8114

S.A. Crowther [a,*], P.L. Clay [a], S. Edwards [a], H. Busemann [b], K.H. Joy [a], A.A. Early [a], R. Burgess [a], A.R. Butcher [c], M. Humayun [d], J.D. Gilmour [a]

[a] Department of Earth and Environmental Sciences, The University of Manchester, UK
[b] ETH Zürich, Institut für Geochemie und Petrologie, Zürich, Switzerland
[c] Geological Survey of Finland GTK, Espoo, Finland
[d] National High Magnetic Field Laboratory and Department of Earth, Ocean and Atmospheric Science, Florida State University, Tallahassee, USA

ARTICLE INFO

Article history:
Received 1 November 2021
Accepted 1 August 2022
Available online 8 August 2022
Associate editor: Christopher Herd

Keywords:
NWA 8114
Mars
Black Beauty
Martian atmosphere
Martian surface

ABSTRACT

The martian meteorite Northwest Africa (NWA) 8114 is a regolith breccia grouped with the NWA 7034 ('Black Beauty') stone and others. The meteorite, with its complex rock and mineral load, records over 4.4 billion years of martian geological and atmospheric history. In this work we present new analyses of noble gases in NWA 8114, and consider the constraints they impose on the evolution of the martian atmosphere over the past 4 billion years. We also report a petrographic overview, halogen abundances, and an argon isotope age, which provide context for interpreting the noble gas data.

The krypton and xenon elemental signature of NWA 8114 is elementally fractionated with respect to the present-day martian atmosphere as measured in shergottite glasses; there is no requirement for a contribution from the ancient martian atmosphere in our data. The xenon isotopic composition incorporates (i) a component enriched in ^{129}Xe (maximum ^{129}Xe/^{132}Xe = 2.450 ± 0.045 compared with a solar ratio of ~ 1), which is similar to the present day martian atmosphere, (ii) a cosmic-ray spallation component dominated by production from barium, and (iii) a fission component. We estimate a cosmic ray exposure (CRE) age of 5.7 ± 1.3 Myr from cosmogenic ^{21}Ne and ^{38}Ar.

Understanding how the martian atmosphere has changed through the planet's history is a key part of understanding the planet's geological history and evolution. We develop a model for the evolution of the martian atmosphere constrained by the amount of spallation-derived xenon in the atmosphere today and the evolution of the ^{129}Xe/^{132}Xe ratio over time. A baseline model in which the early atmosphere collapsed 3.7 Gyr ago (and assuming no further loss) requires a constant degassing of the crustal budget of spallation xenon of 0.034 % Myr^{-1} to accumulate sufficient spallation-derived xenon in the atmosphere. Combining constraints imposed by the ^{129}Xe/^{132}Xe ratio with the spallation budget requires loss of xenon from the martian atmosphere over the last 3.7 Gyr, with the present day budget being as little as 20 % of that at the start of this period.

1. Introduction

The atmospheres of planetary bodies determine the habitability of their surface environments. Present day atmospheres have evolved from those existing at the time of planetary differentiation and crust formation ~ 4.4 billion years (Gyr) ago, through a combination of atmospheric loss and addition of fresh material (e.g., Pollack and Yung, 1980; Zahnle, 1998). Atmospheric loss processes include several thermal and non-thermal processes and stripping by impacts, while new material can be gained from outgassing of the planet's crust or mantle, or by delivery of new material from elsewhere in the solar system, for example, interplanetary dust, asteroids or comets (e.g., Hunten, 1993). Further, atmospheric species could also be re-incorporated into the planetary body interior as a consequence of geological activity. As a result, present day atmospheres may be entirely secondary, with little trace remaining of their primordial compositions. In the case of Mars, observations of features such as valley networks on the surface indicate that the early climate was likely warmer, wetter and characterised by a high carbon dioxide pressure, in contrast to the low-pressure present day atmosphere (e.g., Fanale et al., 1992).

* Corresponding author.
E-mail address: sarah.crowther@manchester.ac.uk (S.A. Crowther).

https://doi.org/10.1016/j.gca.2022.08.002
0016-7037/

Noble gases trace processes of atmospheric evolution because volatile reservoirs in the system have distinct compositional signatures. Noble gases are highly depleted in *rocky* solar system materials, with the lighter elements neon (Ne) and argon (Ar) more strongly depleted relative to their solar abundances than the heavier elements krypton (Kr) and xenon (Xe) (e.g., Pepin, 1991). Helium is lost from the atmospheres of terrestrial planets in our Solar System, and the concentrations and isotopic compositions observed today impose no significant constraints on the origin and long-term evolution of the atmosphere (Pepin, 1991). Excesses of individual isotopes that are produced by radioactive decay from a range of lithophile elements, and on a variety of timescales, are observed in the isotopic signatures of noble gases. Their lack of reactivity leads to noble gases accumulating in atmospheric reservoirs with limited recycling into planetary interiors (e.g., Pepin, 1991; Porcelli and Turekian, 2014). Notably, the nine isotopes of xenon enable us to distinguish contributions from three radioactive progenitors with different characteristic timescales: ^{129}I (producing ^{129}Xe, half-life 16.1 million years (Myr) (Chechev and Sergeev, 2004)), ^{244}Pu (producing ^{131,132,134,136}Xe, half-life 82 Myr (Ozima and Podosek, 2002)), and ^{238}U (also producing ^{131,132,134,136}Xe but with different relative abundances, half-life 4.5 Gyr (Ozima and Podosek, 2002)). Also, distinct xenon isotope signatures have been identified in the sun (solar wind) (Wieler and Baur, 1994; Pepin et al., 1995; Crowther and Gilmour, 2013; Meshik et al., 2014), from primitive meteorites (Busemann et al., 2000), and from the coma of a comet (Marty et al., 2017), allowing contributions from these sources to be traced. In some circumstances, cosmic ray production of xenon isotopes from spallation and secondary neutron capture reactions can be detected.

In this work, we present new analyses of noble gases in the martian regolith breccia Northwest Africa (NWA) 8114 and consider the constraints they provide on the evolution of the martian atmosphere over the past 4 billion years. We examine whether elemental noble gas signatures trapped in martian meteorites are the result of a fractionation process during their incorporation, or whether they represent a change in the elemental composition of the atmosphere over time. We also look at the evolution of the atmosphere as constrained by the xenon isotopic composition of the present-day atmosphere, and that trapped in meteorites at earlier points in martian history. Before examining our data, we briefly review martian noble gas reservoirs and the martian regolith breccias grouped with NWA 8114 to provide context for our data.

1.1. Martian Noble Gas Reservoirs

The martian atmosphere was first analysed *in situ* on the surface of Mars by the Viking spacecraft in the 1970s (Owen et al., 1977); neon, argon, krypton and xenon were detected alongside active species. More recently, the argon, krypton and xenon isotopic compositions have been measured by Mars Science Laboratory's (MSL or 'Curiosity Rover') Sample Analysis at Mars (SAM) instrument (Atreya et al., 2013; Mahaffy et al., 2013; Conrad et al., 2016). The relative abundances of the present-day noble gases are similar to those of Earth's atmosphere, although the surface pressure of the martian atmosphere is less than 1 % that of Earth's atmosphere, and the mass of the martian atmosphere is around 4×10^{-8} of the planetary mass vs 8.5×10^{-7} for the Earth (Mars Fact Sheet). The ^{36}Ar/^{132}Xe and ^{84}Kr/^{132}Xe ratios are $\sim$ 350 and 11, respectively, with uncertainties of $\sim$ 30 % (Owen et al., 1977; Bogard et al., 2001). The present day ^{40}Ar/^{36}Ar ratio, as measured by the Curiosity Rover, is 1900 ± 300 (Mahaffy et al., 2013), while the ^{38}Ar/^{36}Ar ratio is 0.238 ± 0.006 (Atreya et al., 2013) (both 1σ uncertainties). Both these ratios are higher than the terrestrial atmospheric values (298.56 ± 0.31 and 0.1885 ± 0.0003 respectively (Lee et al., 2006)), a consequence of the more substantial atmospheric loss on Mars relative to Earth. Modelling of data from the Mars Atmosphere and Volatile Evolution (MAVEN) spacecraft requires 66 % of the ^{36}Ar that was ever in the martian atmosphere to have been lost to space (Jakosky et al., 2017). The isotopic composition of present-day martian atmospheric krypton is consistent with solar krypton modified by a contribution to ^{80}Kr and ^{82}Kr from neutron capture on bromine (Conrad et al., 2016). The xenon isotopic composition is fractionated relative to solar xenon, with a large ^{129}Xe excess from decay of ^{129}I: the ^{129}Xe/^{132}Xe ratio was determined to be 2.5221 ± 0.0063 (1σ uncertainty) (Conrad et al., 2016), compared to a solar ratio of $\sim$ 1 (Crowther and Gilmour, 2013; Meshik et al., 2014). A contribution from spallation xenon is apparent in the light isotopes. Excesses in ^{131}Xe, attributed to neutron capture on ^{130}Ba, are observed, whereas contributions to ^{128}Xe from neutron capture on ^{127}I appear to be minor.

Shergottites are the most abundant and most diverse group of martian meteorites, commonly subdivided into basaltic, olivine-phyric and poikilitic subgroups based on their mineralogy. The elemental abundances and isotopic ratios of noble gases trapped in impact glasses in shergottite meteorite samples, in particular Elephant Moraine A79001 (EETA79001), showed notable similarities to the present day martian atmosphere (Bogard and Johnson, 1983; Wiens et al., 1986; Wieler et al., 2016; Avice et al., 2018). It is thought that these atmospheric gases were trapped in the impact glasses by shock events (Bogard and Johnson, 1983). Studies have shown that shock implantation of noble gases does not significantly fractionate the elemental or isotopic composition (Bogard et al., 1986; Wiens and Pepin, 1988). Most shergottites have crystallisation ages < 200 million years (Ma), although ages range up to 600 Ma, and they were all shocked and ejected from the martian surface within the past 20 Myr (Udry et al., 2020). The impact glasses must have formed no earlier than the crystallisation age, but possibly as late as the time of the ejection event(s). This implies that the martian atmospheric component must have been incorporated more recently than < 200 Ma, sampling the relatively recent martian atmosphere (Garrison and Bogard, 1998). The isotopic composition measured in shergottites can, however, be complicated by spallation contributions (e.g., Becker and Pepin, 1984; Swindle et al., 1986), and the calculated isotopic composition of the martian atmosphere can depend on the compositions adopted for other isotopic end-members (e.g., Wiens et al., 1986).

^{129}Xe and ^{136}Xe provide key constraints on the evolution of noble gas reservoirs (Fig. 1). Swindle et al. (1986) suggested a ^{129}Xe/^{132}Xe ratio of 2.40 ± 0.02 for a martian atmosphere component trapped in EETA79001 shergottite glass. Bogard and Garrison (1998) subsequently measured a maximum ^{129}Xe/^{132}Xe ratio of 2.59 ± 0.03 in an individual heating step in a separate aliquot of the same EETA79001 glass – this is slightly higher than the Curiosity Rover measured for the martian atmosphere. All values show a significant contribution from ^{129}I decay over a baseline ^{129}Xe/^{132}Xe of around 1 in solar system xenon reservoirs such as solar wind (Crowther and Gilmour, 2013; Meshik et al., 2014) and Q-Xe (Busemann et al., 2000). ^{136}Xe/^{132}Xe ratios of 0.3514 ± 0.0015 and 0.3533 ± 0.0047 are reported for these EETA79001 glass samples (Swindle et al., 1986; Garrison and Bogard, 1998), and a ratio of 0.3451 ± 0.0023 was measured by the Curiosity Rover (Conrad et al., 2016). The ^{136}Xe/^{132}Xe ratio can be accounted for by mass fractionation of an underlying solar wind component; there appears to be no conclusive evidence for a fission component in the heavy isotopes. (Although depending on the choice of starting compositions, a small fission contribution may be present (Conrad et al., 2016; Pepin, 2000; Swindle and Jones, 1997)). ^{36}Ar/^{132}Xe and ^{84}Kr/^{132}Xe ratios (Fig. 2) have been determined to be 900 ± 100 and 20.5 ± 2.5 respectively for the EETA79001 shergottite glasses (Bogard and Garrison, 1998) – somewhat higher than the Viking

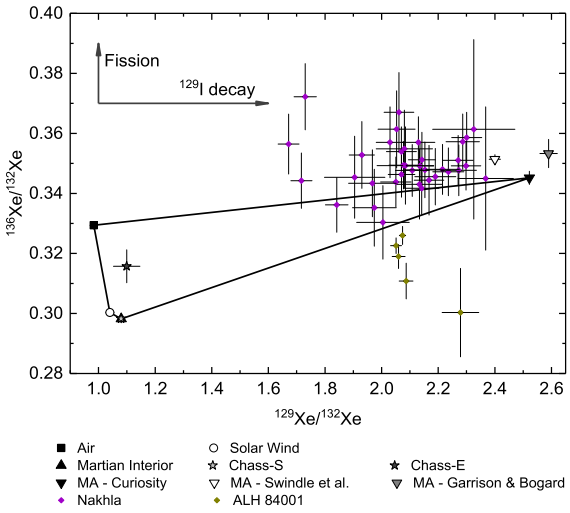

Fig. 1. Several xenon components are found in martian meteorites: (1) a martian atmosphere (MA) component characterised by an elevated $^{129}Xe/^{132}Xe$ ratio (compared to values close to 1 for solar system reservoirs such as the terrestrial atmosphere (Basford et al., 1973) and solar wind (Crowther and Gilmour, 2013)); (2) components derived from reservoirs in the martian interior, which include a solar xenon reservoir and a source of xenon from spontaneous fission of ^{244}Pu (Chass-S and Chass-E, (Mathew and Marti, 2001)); (3) fission components produced *in situ* by spontaneous fission of ^{244}Pu and/or ^{238}U; (4) spallation components produced from reactions of cosmic rays with barium and/or rare earth elements (REE); and (5) terrestrial contamination. The $^{129}Xe/^{132}Xe$ ratio of the martian atmosphere (MA) is ~ 2.5, as measured by Curiosity (Conrad et al., 2016), and determined from EETA79001 glass by Swindle et al. (1986) and Garrison and Bogard (1998), indicating a significant contribution from ^{129}I decay. The $^{129}Xe/^{132}Xe$ ratio of the martian atmosphere component in Nakhla is calculated to be 2.350 ± 0.026 (Gilmour et al., 2001), which is a little lower than that seen by Curiosity or in EETA79001. Selected data for ALH 84001 (Swindle et al., 1995; Gilmour et al., 1998; Mathew and Marti, 2001) illustrate the lower $^{129}Xe/^{132}Xe$ and $^{136}Xe/^{132}Xe$ ratios of the ancient martian atmosphere are not consistent with mixing of martian interior and present day atmosphere. Error bars that are not visible are smaller than the symbols used.

measurements (Owen et al., 1977; Bogard et al., 2001). It seems unlikely that these ratios would have changed significantly in the < 200 Ma between shergottite crystallisation and subsequent formation of the impact glasses, and the Viking measurement, and it is thought that the shergottite data are probably a more accurate representation of the recent Martian atmosphere (Bogard et al., 2001).

There are only three known Chassignites at the time of writing (Meteoritical Bulletin Database). They are dunites formed from basaltic magmas (McSween and Treiman, 1998), and the distinct noble gas signature of Chassigny has been associated with the martian interior (Ott, 1988). The composition of xenon released from Chassigny in step pyrolysis experiments varies with release temperature, suggesting there are two components: Chass-S and Chass-E (Mathew and Marti, 2001) (Fig. 1). Chass-S, released at lower temperature, has a *solar* signature; Chass-E is an *evolved* component, which appears to be related to Chass-S by addition of ^{244}Pu-derived fission xenon. Chass-E has a uniform isotopic signature, implying that the fission component was well mixed with the solar component before incorporation into the rock (Chassigny crystallised at ~ 1.3 Ga, the same time as the nakhlites (Nyquist et al., 2001), ruling out *in situ* decay of ^{244}Pu). Both components have relatively low $^{129}Xe/^{132}Xe$ ratios (~1.07). The $^{36}Ar/^{132}Xe$ and $^{84}Kr/^{132}Xe$ ratios of Chass-S are constrained to be < 5 and < 1.1 respectively, those of Chass-E are greater than 130 and greater than 1.8, both of which are distinct from the martian atmosphere ratios (Mathew and Marti, 2001) (Fig. 2).

The $^{84}Kr/^{132}Xe$ and $^{129}Xe/^{132}Xe$ ratios in Chassigny and most shergottites are thought to define a mixing line between the martian atmosphere and interior components. Nakhla, however, has low $^{36}Ar/^{132}Xe$ and $^{84}Kr/^{132}Xe$ ratios relative to its $^{129}Xe/^{132}Xe$ ratio (i.e. the $^{36}Ar/^{132}Xe$ and $^{84}Kr/^{132}Xe$ ratios are lower than expected based on the $^{129}Xe/^{132}Xe$ ratio, and data plot to the left of the mixing line in Fig. 2). The low elemental ratios are thought to represent elementally fractionated martian atmosphere (Ott, 1988; Drake et al., 1994; Bogard and Garrison, 1998). The $^{129}Xe/^{132}Xe$ ratio of the martian atmosphere component in Nakhla is calculated to be 2.350 ± 0.026, based on a mixing line with spallation xenon (Gilmour et al., 2001). The atmospheric xenon component is associated with acid leachable iodine, indicating it is likely to be sited close to grain surfaces (Gilmour et al., 2001). Dissolution of iodine in a water soluble phase is ruled out because xenon and iodine are correlated in water treated samples. The location of iodine close to grain surfaces, combined with the fractionation of krypton from xenon in the martian atmospheric component in Nakhla (Drake et al., 1994; Bogard and Garrison, 1998), has led to the suggestion that shock implantation of surface adsorbed atmospheric gases is the most likely mechanism by which xenon and krypton were incorporated into Nakhla (Gilmour et al., 2001). A shock event at 630 Myr affecting the nakhlite meteorites has recently been reported by Daly et al. (2019). The cosmic ray exposure ages of both nakhlites and chassignites are ~ 11 Ma, making in plausible that they were ejected from the surface by a single event (Herzog and Caffee, 2014). In contrast, the shergottites have a range of cosmic ray exposure ages, that require several ejection events (Herzog and Caffee, 2014).

Allan Hills (ALH) 84001 is a unique martian meteorite, an orthopyroxenite that is not assigned to one of the SNC groups. It is significantly older than other known martian meteorites, with a crystallisation age of ~ 4.1 billion years (Ga) (Bouvier et al., 2009; Jagoutz et al., 2009; Lapen et al., 2010). Ar-Ar ages of ALH 84001 range from ~ 4.1 Ga, identical to the crystallisation age, to around 3.9 Ga (Ash et al., 1996; Bogard and Garrison, 1999; Cassata et al., 2010; Turner et al., 1997). The younger age is attributed to a major shock event which reset the Ar-Ar chronometer (Turner et al., 1997). The spread of ages is thought to be due to heterogeneous heating of the ALH 84001 source material during this shock event (Cassata et al., 2010). Similar to Nakhla, argon and krypton in ALH 84001 are depleted relative to xenon and the $^{36}Ar/^{132}Xe$ and $^{84}Kr/^{132}Xe$ ratios are distinct from those of the present day martian atmosphere (Mathew and Marti, 2001) (Fig. 2). The $^{129}Xe/^{132}Xe$ ratio of the trapped component is significantly lower than that of the present day martian atmosphere; different authors report values between 1.95 ± 0.18 (Gilmour et al., 1998) and 2.17 ± 0.04 (Mathew and Marti, 2001). Furthermore, combined with the $^{136}Xe/^{132}Xe$ ratio, the xenon isotope signature is not consistent with that expected from mixing of martian interior and present-day martian atmosphere components, and shows no evidence for *in situ* decay of ^{244}Pu or ^{129}I (Fig. 1). The underlying signature of the xenon isotopic composition was originally interpreted to be unfractionated solar xenon (in contrast to the fractionated signature seen in the present day atmosphere) (Mathew and Marti, 2001). More recent work suggests the xenon isotopic signature is fractionated by a similar extent as the present-day atmosphere, albeit with a lower $^{129}Xe/^{132}Xe$ ratio (Cassata, 2017). Nevertheless these observations suggest that the trapping event occurred at least 4 Gyr ago (Gilmour et al., 1998), and sampled the ancient 4 Ga martian atmosphere before it had evolved to its present xenon isotopic composition.

1.2. Martian Regolith Breccias NWA 7034 and its pairs

The Northwest Africa (NWA) 7034 ('Black Beauty') meteorite (Agee et al., 2013) and grouped stones NWA 7475 (Wittmann et al., 2015), NWA 7533 (Humayun et al., 2013; Hewins et al.,

2017), NWA 7906 (Hofmann et al., 2014), NWA 7907 (Hofmann et al., 2014), NWA 8114 (Griffiths et al., 2014; MacArthur et al., 2019), NWA 8171 (Hofmann et al., 2014), NWA 8674, NWA 10922 (Habermann et al., 2017), NWA 11220, NWA 11522 (Cohen et al., 2018), NWA 11896, NWA 11921, NWA 12222, NWA 13561, Rabt Sbayta 003, Rabt Sbayta 010 and Rabt Sbayta 012 are dark-coloured, polymict breccia martian meteorites with a combined mass of just under 1 kg (Meteoritical Bulletin Database). The samples are lithologically distinct from the other martian meteorites, which are igneous rocks. The samples are typically heterogeneous stone to stone, but have shared characteristics, including a typically fine-grained matrix derived from altered basaltic mineral fragments and diverse lithic clast compositions (Humayun et al., 2013; Santos et al., 2015). The samples contain rare phyllosilicates (Muttik et al., 2014) and a variety of Fe oxides including maghemite and magnetite (Beck et al., 2015) indicating that the source materials experienced aqueous alteration. The meteorites' mineralogy and chemistry suggest they are representative of a source region on Mars similar to basaltic regolith in low albedo (dust-poor) dark plains areas (Humayun et al., 2013; Cannon et al., 2015). Several studies (e.g., Humayun et al., 2013; Santos et al., 2015) have suggested that the bulk composition of this group of meteorites most closely match the rocks in Gusev Crater, as analysed by the Mars Exploration Rover Spirit (Gellert et al., 2004, 2006; Yen et al., 2005).

Old U-Pb ages of zircon crystals in NWA 7034 and NWA 7533, at ~ 4.44–4.43 Ga, provide evidence for early martian crustal differentiation (Humayun et al., 2013; Nemchin et al., 2014). A second group of ancient zircons suggests NWA 7034 records at least two igneous events between 4.44 and 4.35 Ga (Yin et al., 2014). Rb-Sr dating of the bulk rock yielded ages ~ 2.1 Ga in the Amazonian epoch (Agee et al., 2013), but evidence of disturbance of the Rb-Sr system and a Sm-Nd mineral isochron of 4.39 Ga (Nyquist et al., 2016) establishes an older age for most of the breccia components. Younger zircon and phosphate U–Pb ages of 1.7 Ga (Nemchin et al., 2014) and 1.4–1.3 Ga (Yin et al., 2014; Bellucci et al., 2015) could represent the final assembly of the breccia, a late stage impact, or a magmatic resetting event (Bellucci et al., 2015). K-Ar ages of ~1.6 Ga (Cartwright et al., 2014; Stephenson et al., 2017), and the Ar-Ar ages of ~ 1.3 Ga recorded in NWA 7034 (Cassata et al., 2018) and ~ 1.4 Ga in NWA 7533 (Lindsay et al., 2021), are all probably related to resetting during one or more impact-related heating events (Cassata et al., 2018). Lindsay et al. (2021) suggest that these Ar-Ar ages of the breccia are similar enough to the crystallisation ages of the nakhlite-chassignite suite to warrant the possibility of contact metamorphism of the breccia at ~ 1.4 Ga by the nakhlite intrusives. However, distinct cosmic ray exposure (CRE) ages (Herzog and Caffee, 2014) exclude ejection upon the same impact. A U/Th-He age of ~ 170 Ma has been reported, which is similar to the crystallisation ages of shergottites (Nyquist et al., 2001), perhaps hinting at a comparable thermal history (Cartwright et al., 2014). Cassata et al. (2018) report slightly younger U-Th-Sm/He ages of ~ 135 and ~ 133 Ma, and suggest the differences are due to incomplete degassing of ^{4}He during metamorphic events, brecciation and/or ejection. They also suggest that the U-Th-Sm/He ages constrain the time of brecciation to no earlier than 225 Ma (Cassata et al., 2018).

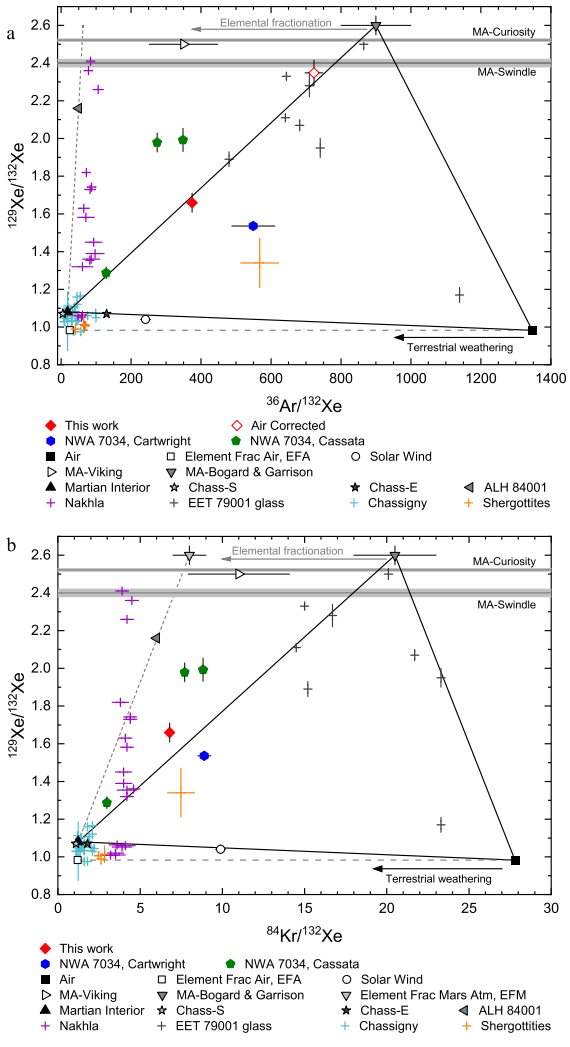

Fig. 2. Standard plot of (a) ^{129}Xe/^{132}Xe vs ^{36}Ar$_{tr}$/^{132}Xe and (b) ^{129}Xe/^{132}Xe vs ^{84}Kr/^{132}Xe (Table 1). The ^{36}Ar$_{tr}$/^{132}Xe and ^{129}Xe/^{132}Xe ratios for our datum for NWA 8114 plots on the mixing line between modern martian atmosphere (Bogard and Garrison, 1998) and a component consistent with the martian interior (Mathew and Marti, 2001) or with elementally fractionated terrestrial atmosphere (EFA, (Mohapatra et al., 2009; Mohapatra et al., 2002)). The ^{129}Xe/^{132}Xe vs ^{84}Kr/^{132}Xe point lies to the left of a mixing line between the martian interior component and the modern atmosphere. This is likely due to elemental fractionation of one or both of martian or terrestrial atmosphere during their incorporation into the host rock. The 'Air Corrected' point in (a) shows how the ^{36}Ar$_{tr}$/^{132}Xe and ^{129}Xe/^{132}Xe ratios change if corrected for a 51 % contribution to ^{132}Xe from terrestrial air, based on modelling of the data that also incorporated modern martian atmosphere, fission and spallation components (Section 3.2). Data for NWA 7034 (Cartwright et al., 2014; Cassata, 2017) are plotted as the total gas released from each sample, for direct comparison with our single step analysis. Nakhla (Mathew and Marti, 2002), Chassigny (Mathew and Marti, 2001), EETA79001 glass (Bogard and Garrison, 1998), and the ancient martian atmosphere determined from ALH 84001 (Mathew and Marti, 2001) are shown for comparison. Examples of shergottites LAR 06319, 12011, 12095, and 12240 show evidence of the EFA component (Clay et al., 2020). Additional literature values are also shown for the terrestrial atmosphere (Basford et al., 1973), the martian atmosphere (MA) as measured by Viking (Owen et al., 1977; Bogard et al., 2001), Curiosity (Conrad et al., 2016) and in shergottite glasses (Swindle et al., 1986; Bogard and Garrison, 1998), and solar wind (Vogel et al., 2011). Direct measurements of the elemental ratios were not made by Swindle et al. (1986) or Curiosity, so the range of the ^{129}Xe/^{132}Xe ratios are shown as grey bars. The ratios plotted for Chass-S are the lowest ^{36}Ar/^{132}Xe and ^{84}Kr/^{132}Xe ratios measured in SNC meteorites, and represent an upper limit for the component (Mathew and Marti, 2001). Chass-E is related to Chass-S by addition of ^{244}Pu-derived xenon (Fig. 1); the values plotted here represent a lower limit for the ^{36}Ar/^{132}Xe and ^{84}Kr/^{132}Xe ratios (Mathew and Marti, 2001). Schwenzer and Ott (2006) estimate a ^{84}Kr/^{132}Xe ratio of 8 ± 1 for elementally fractionated martian atmosphere (EFM) endmember. The dashed gray line indicates mixing between terrestrial air and elementally fractionated air. The dotted grey line in (b) indicates mixing between the martian interior component and EFM endmember, which passes through the ALH 84001 datum; a similar line is drawn in (a) from the martian interior component, passing through the ALH 84001 datum, to the martian atmosphere ^{129}Xe/^{132}Xe ratio. Error bars that are not visible are smaller than the symbols used, with the exception of the ^{129}Xe/^{132}Xe ratio measured by Viking, which has an uncertainty of ± 2 that is not shown for scale.

Two studies have examined the noble gas composition of NWA 7034, but have drawn different conclusions. The first study reported $^{36}Ar/^{132}Xe$ and $^{84}Kr/^{132}Xe$ ratios within the range of other martian meteorites, and a maximum $^{129}Xe/^{132}Xe$ ratio of 1.725 ± 0.14 for a single heating step (Cartwright et al., 2014). The trapped component is most likely elementally fractionated modern martian atmosphere, and xenon data are consistent with mixing of the modern martian atmosphere with a martian interior component. In contrast, a more recent study argues that the $^{36}Ar/^{132}Xe$, $^{84}Kr/^{132}Xe$ and $^{129}Xe/^{132}Xe$ ratios contain a trapped component consistent with that identified in ALH 84001, i.e. an ancient martian atmosphere component (Cassata, 2017). Maximum $^{129}Xe/^{132}Xe$ ratios of ~ 2.1–2.2 are reported, which are indistinguishable from the $^{129}Xe/^{132}Xe$ ratio found in ALH 84001 (Gilmour et al., 1998; Mathew and Marti, 2001). The $^{36}Ar/^{132}Xe$ and $^{84}Kr/^{132}Xe$ ratios of this component also appears consistent with the trapped component of ALH 84001 mixing with terrestrial atmosphere. These observations are interpreted to suggest that the trapped components in ALH 84001 and NWA 7034 are elementally and isotopically similar (Cassata, 2017).

In this study, we present new analyses of the noble gas composition in NWA 8114, and consider the implications for the evolution of the martian atmosphere over the past 4 billion years. We examine whether the $^{36}Ar/^{132}Xe$ and $^{84}Kr/^{132}Xe$ elemental signatures require a change in the elemental composition of the atmosphere over time, or whether they are the result of a fractionation process during their incorporation into the host rock. We also investigate the xenon isotopic composition and look at how the evolution of the martian atmosphere can be constrained by the xenon isotopic composition recorded in ALH 84001 (Gilmour et al., 1998; Mathew and Marti, 2001), Nakhla (Gilmour et al., 2001) and NWA 8114, and the present day composition of the martian atmosphere as measured by Curiosity Rover (Conrad et al., 2016).

2. Experimental methods

The petrology of NWA 8114 is described in detail in MacArthur et al. (2019); characterisation of our sample of NWA 8114 is discussed in detail in the Supplementary Information (Section S3.1). Briefly, preliminary analysis was carried out using a computerised X-ray computed tomography (CT) scanner (Nikon custom Bay at the Manchester X-ray Imaging Facility (MXIF)), the sample was characterised by optical and electron microscopy (Phillips FEI XL30 Environmental Scanning Electron Microscope-Field Electron Gun (ESEM-FEG) at the University of Manchester), major and minor elemental concentrations were obtained by Electron Probe Micro-Analyser analysis (Cameca SX-100 at the University of Manchester), and the modal mineralogy of NWA 8114 was calculated using QEMSCAN modal phase analysis (QEMSCAN® 4300 at the Camborne School of Mines, University of Exeter). Following the preliminary characterisation, material was selected for noble gas, xenon and halogen analysis, and Ar-Ar dating. In this work our focus is on the evolution of the martian atmosphere as recorded by noble gases, so we discuss the noble gas and xenon analyses in detail here. Ar-Ar dating and halogen analyses are reported and discussed in the Supplementary Information. In addition to the xenon isotopic analyses discussed here, a further two samples were artificially neutron irradiated in a nuclear reactor prior to analysis of the xenon composition, in an attempt to examine isotopes of xenon produced from neutron capture by ^{127}I (^{128}Xe) and ^{130}Ba (^{131}Xe), and neutron-induced fission of ^{235}U ($^{131\text{-}136}Xe$). These analyses were dominated by iodine- and barium-derived xenon and are available in the online Research Data.

2.1. Total Fusion Noble Gas Analysis

The isotopes of all the noble gases, helium to xenon, were analysed at ETH Zürich by fusing a bulk sample (62.63 ± 0.02 mg) taken from three chips of NWA 8114. The samples were analysed according to standard procedures described in detail by Riebe et al. (2017). The sample was extracted in a single heating step at 1700 °C; a further, higher temperature step contained no gas. Blank corrections (determined in empty aluminium packages, but otherwise measured identically to the sample) were ≤ 0.2 % of the measured gas for $^{3,4}He$, $^{21,22}Ne$, ≤1.2 % for ^{20}Ne, $^{38,40}Ar$, ~3 % for ^{36}Ar, 0–7 % for the krypton, and 0–10 % for the xenon isotopes.

2.2. Xenon Isotope Analysis

The xenon concentrations and isotopic compositions were analysed using the RELAX (Refrigerator Enhanced Laser Analyser for Xenon) mass spectrometer (Gilmour et al., 1994; Crowther et al., 2008). Two single chips of rock from split 6a, which originated from the centre of our sample and had no fusion crust (samples labelled NWA8114_6a_1 and NWA8114_6a_2, with masses 2.56 and 1.52 mg, respectively), were analysed alongside a third sample which comprised 4 grains of matrix cuttings, i.e., material left over from the Sample 0 cutting process (labelled NWA8114_133, total mass 1.33 mg) – see Fig. S2 for details of how the sample was split.

The samples were step-heated with a continuous wave Nd:YAG laser (λ = 1064 nm), with each step of 1 min duration, at a series of sequentially increasing powers. The gas extracted in each heating step was gettered (sintered Zr, ~350 °C) for one minute to remove active gases before being admitted into the RELAX mass spectrometer. Gas in the mass spectrometer is continually condensed on a localised cold spot, and is released every 0.1 s by pulses from an infrared laser (λ = 1064 nm, 5 mJ, 10 ns pulse). The ionising laser (λ = 249.6 nm, 2 mJ) is then fired through the resulting plume of gas when its concentration in the ionising region reaches a maximum, selectively ionising xenon. The xenon isotopes are separated according to mass by the time-of-flight analyser, and microchannel plate detectors allow for the detection of all xenon isotopes from each laser pulse.

Data were acquired from 3,000 consecutive condensation-release-ionisation cycles over a period of 5 min. These were summed over 10 s intervals to produce 30 mass spectra, each of which corresponds to the integrated signal detected in that period. Scatter of the isotope ratios derived from these data around an evolution line was used to determine the measurement uncertainty (Crowther et al., 2008). In this work, the sum of the first 5 summed spectra (first 50 s of data collection) was used to determine isotope ratios and errors, and the signal intensity of a normalising isotope. Sample analyses were interspersed with air calibrations and procedural blanks. Air calibrations enable a correction for instrument dependent mass fractionation, and for the absolute quantities of gas to be calculated. The procedural blank ranged between ~ 1400 and ~ 2500 atoms ^{132}Xe during these analyses, and a blank correction has been applied to the data presented here. 1σ uncertainties are quoted for all xenon data.

3. Results

The mineralogy and petrology of our sample of NWA 8114 is discussed in detail in the Supplementary Information (Section S3.1). Briefly, it is a polymict regolith breccia (Figs. S3 and S4) that contains multiple mineral fragments and a range of polymineralic clasts surrounded by a fine-grained matrix. It is predominantly composed of calcic pyroxene and feldspar, with a range of accessory phases including chlorapatite, magnetite, ilme-

nite, chromite, calcite (as secondary veins), zircon and pyrrhotite (Fig. S4 and Table S5). Our sample is consistent with the texture and mineralogy of NWA 8114 reported by MacArthur et al. (2019), and those of NWA 7034 and grouped stones (e.g., Agee et al., 2013; Humayun et al., 2013).

The aliquots chosen for argon-argon dating, noble gas, halogen and two of the xenon analyses were small chips from the centre of the sample with no fusion crust, and are indicated in Fig. S2. They were broadly representative of the bulk sample, but the heterogeneity of NWA 8114 on a mm-scale (Fig. S1, Fig. S4) means that individual sub-splits selected for these analyses will likely be very dependent on the specific split being analysed (i.e., clast rock type, clast size, mineral content, terrestrial weathering veins). The third sample analysed for xenon isotopes comprised grains of material left over from the sample splitting process and was likely dominated by matrix.

Argon-argon dating and halogen results are discussed in detail in the Supplementary Information. Ar-Ar step release ages are between 1012 and 1370 Ma with an apparent isochron age of 1385 ± 21 Ma (Section S3.2). Halogen concentrations of 1410 ± 110 ppm chlorine, 1800 ± 210 ppb bromine and 1930 ± 140 ppb iodine were determined, which correspond to Br/Cl and I/Cl ratios of $(1.3 \pm 0.2) \times 10^{-3}$ and $(1.4 \pm 0.2) \times 10^{-3}$, respectively (Section S3.4).

3.1. Noble Gas Abundances and elemental ratios

Table 1 presents concentrations and ratios of the noble gases measured in a single release step by fusing the bulk, 62.63 mg sample of NWA 8114 at ETH Zürich. The noble gas concentrations are broadly consistent with those reported for NWA 7034 (Cartwright et al., 2014; Cassata et al., 2018). The helium, neon and argon isotopic compositions are mixtures of radiogenic (^{4}He, ^{40}Ar), cosmogenic (^{3}He, all Ne isotopes, ^{38}Ar) and minor amounts of trapped components (best visible in ^{36}Ar), again generally consistent with similar analyses of NWA 7034 (Cartwright et al., 2014; Cassata et al., 2018).

The $^{36}Ar_{tr}/^{132}Xe$ and $^{129}Xe/^{132}Xe$ ratios plot on the mixing line between the modern martian atmosphere and a component consistent with the martian interior or elementally fractionated terrestrial atmosphere (EFA, Mohapatra et al., 2002, 2009) (Fig. 2a). The data point of the bulk sample in the $^{129}Xe/^{132}Xe$ vs $^{84}Kr/^{132}Xe$ plot (Fig. 2b) plots to the left (low $^{84}Kr/^{132}Xe$) of a mixing line between the modern martian atmosphere and the martian interior or EFA. This could be due to either a contribution from the ancient martian atmosphere or elemental fractionation; it is discussed further in Section 4.3.1.

3.2. Xenon Isotopes

The xenon isotopic composition for the single-step extraction of this sample measured at ETH (Table 1) was modelled as a combination of components plausibly expected to be present in the sample using the methodology described in Crow et al. (2020) (Table S1). Contributions were allowed from the modern martian atmosphere, terrestrial air, spallation of barium and rare earth elements, and fission of ^{244}Pu and ^{238}U. These components are consistent with the mineralogy of NWA 8114 (Table S5): K-feldspar contains barium, and both chlorapatite and zircon incorporate rare earth elements. Zircon also contains uranium, and the old U-Pb ages of zircon crystals identified in paired stones NWA 7034 and NWA 7533 (Humayun et al., 2013; Nemchin et al., 2014; Bouvier et al., 2018; Costa et al., 2020) allow for the incorporation of live ^{244}Pu (half-life 82 Ma) at the time of crystallisation (as has been detected in ancient terrestrial zircons (Turner et al., 2004)). If χ^2 per degree of freedom of this maximum likelihood model was < 2, the model was deemed to account for the data – the observed xenon composition can be accounted for by the expected components, or a subset of them. If a successful fit cannot be achieved either another component is present or a process not accounted for in the model has occurred. ^{131}Xe was not included in the calculation of χ^2 because the production rate arising from secondary neutron capture on ^{130}Ba depends on burial depth during cosmic ray exposure. ^{128}Xe is potentially produced after secondary neutron capture on ^{127}I; a fit including ^{128}Xe was acceptable (χ^2 per degree of freedom was 1.6) but called for an approximately 2σ excess in this isotope; while a fit excluding this isotope yielded χ^2 per degree of freedom of 0.2 (Table S1). The ETH data are given as isotope ratios to ^{132}Xe rather than atoms per isotope, so uncertainty in the measurement of ^{132}Xe is included in each ratio contributing to the fit; this leads to an underestimate of χ^2. Thus there is some evidence of production of ^{128}Xe from ^{127}I through capture of secondary neutrons generated by cosmic rays.

Since an acceptable fit was possible there is no need in these data for components other than those included in the model, although that does not categorically rule them out. Acceptable fits call for a 42–43 % contribution to ^{132}Xe from modern martian atmosphere, with a 50–52 % contribution from terrestrial air (Table S1). There is a 9–10 % contribution to ^{136}Xe from fission of either ^{244}Pu or ^{238}U, but it is not possible to determine which parent is responsible. There is a 25–30 % contribution to the spallation signature at ^{126}Xe from rare earth elements. Correcting the $^{36}Ar_{tr}/^{132}Xe$ and $^{129}Xe/^{132}Xe$ ratios for a 51 % contribution from terrestrial air to the measured ^{132}Xe moves the point much closer to the modern martian atmosphere composition in Fig. 2a. The krypton isotopic signature can be accounted for in a similar way, with a small contribution of ^{80,82}Kr from neutron capture on bromine isotopes.

Turning to the step heating analyses conducted using the RELAX mass spectrometer, xenon data for the two samples of split 6, and the sample of matrix cuttings analysed are summarised in Table 2, and full data with isotope ratios from individual heating steps are given in Table S2. Data from heating steps with uncertainties of the ratios of the major isotopes $\leq$ 5 % of the measured values are illustrated in Fig. 3 to Fig. 5. The three samples gave consistent results, they have similar concentrations of ^{132}Xe and the isotope ratios show the same trends of evolution with increasing temperature across the three samples. The concentrations of excess ^{129}Xe (over a solar ratio of 1) are within a factor of 2.2 or less of the bulk sample (Table 1) and the concentrations reported for NWA 7034 (Cartwright et al., 2014; Cassata, 2017); any differences are likely due to the heterogeneity of samples and the different masses of material analysed. Measured $^{129}Xe/^{132}Xe$ ratios are high, up to $\sim$ 2.4 (Fig. 4 and Table S2). $^{134}Xe/^{132}Xe$ and $^{136}Xe/^{132}Xe$ show a general increase with increasing temperature (corresponding to an increasing contribution from fission) (Fig. 5), as do the $^{124}Xe/^{132}Xe$ and $^{126}Xe/^{132}Xe$ ratios (contribution from spallation) (Fig. 3 and Fig. 4).

As earlier, xenon data from individual step releases were modelled as mixtures of components reasonably expected using the approach detailed in Crow et al. (2020) (Table S3). ^{128}Xe may be produced by secondary neutron capture on ^{127}I and there is some evidence of its presence in the total fusion result, so this isotope was excluded from the calculation of χ^2 and monitored as an excess over the composition predicted from the best fit model (RELAX can also exhibit an interference at mass 128 due to non-resonant ionisation of hydrocarbons (Crowther et al., 2008)). Once again ^{131}Xe was excluded because secondary neutrons derived from the cosmic ray flux cause the $^{131}Xe/^{126}Xe$ ratio associated with barium spallation to vary with depth during exposure.

Table 1
Noble gas data for a single, 62.63 (2) mg sample of NWA 8114 measured at ETH Zürich. The subscript t refers to the trapped component, and c to the cosmogenic component.

$^{3}He_c$ ($\times 10^{-8}$ cm^3 STP g^{-1})	^{4}He ($\times 10^{-8}$ cm^3 STP g^{-1})	$^{3}He/^{4}He$	^{20}Ne ($\times 10^{-8}$ cm^3 STP g^{-1})	$^{21}Ne_c$ ($\times 10^{-8}$ cm^3 STP g^{-1})	$^{20}Ne/^{22}Ne$	$^{21}Ne/^{22}Ne$
3.8436 (85)	1265.3 (4.7)	0.003038 (13)	1.641 (15)	1.411 (13)	0.9083 (24)	0.7807 (27)

^{36}Ar ($\times 10^{-8}$ cm^3 STP g^{-1})	^{40}Ar ($\times 10^{-8}$ cm^3 STP g^{-1})	$^{36}Ar/^{38}Ar$	$^{40}Ar/^{36}Ar$	$^{36}Ar_t$ ($\times 10^{-8}$ cm^3 STP g^{-1})	$^{38}Ar_c$ ($\times 10^{-8}$ cm^3 STP g^{-1})	$^{36}Ar_t/^{132}Xe$
1.566 (28)	2091 (62)	1.751 (14)	1335 (31)	1.146 (49)	0.646 (43)	362(17)

^{84}Kr ($\times 10^{-10}$ cm^3 STP g^{-1})	$^{74}Kr/^{84}Kr$	$^{80}Kr/^{84}Kr$	$^{82}Kr/^{84}Kr$	$^{83}Kr/^{84}Kr$	$^{86}Kr/^{84}Kr$	$^{84}Kr/^{132}Xe$
2.059 (55)	0.01555 (32)	0.1158 (18)	0.2615 (38)	0.2575 (42)	0.2965 (47)	6.51(21)

^{132}Xe ($\times 10^{-10}$ cm^3 STP g^{-1})	$^{124}Xe/^{132}Xe$	$^{126}Xe/^{132}Xe$	$^{128}Xe/^{132}Xe$	$^{129}Xe/^{132}Xe$	$^{130}Xe/^{132}Xe$	$^{131}Xe/^{132}Xe$	$^{134}Xe/^{132}Xe$	$^{136}Xe/^{132}Xe$
0.3162 (60)	0.02802 (66)	0.0435 (12)	0.1378 (40)	1.652 (33)	0.1773 (46)	0.868 (24)	0.398 (13)	0.3515 (90)

Uncertainties are 1 σ, and are given in the units of the last significant figure(s).
Production rates are determined based on the physical model predictions for ordinary chondrites* (Leya and Masarik, 2009, and updates), the bulk target element chemistry given for NWA 7034 (Agee et al., 2013) and the measured purely cosmogenic $^{21}Ne/^{22}Ne$ used as shielding indicator, which suggests a most likely pre-atmospheric radius of ~20 cm. We consider further "allowed" shielding conditions (Mertens et al., 2021), with radii ≥50 cm and sample depths of >~30 cm highly unlikely. This would suggest a pre-atmospheric radius of the NWA 7034 clan meteoroid of ~1.7 t. The total mass of ~940 g of all NWA 7034 clan rocks would yield a sphere of ~4 cm radius.
*A comparison of a model for shergottites and ordinary chondrites (Krietsch, 2020; Wieler et al., 2016) yields no significant matrix effects. However, as the shergottite model calculations cover only small meteoroids with ≤7 cm radius, we used here the OC model for radii 10–500 cm.
We obtain production rate ranges (in cm^{3}g^{-1}Myr^{-1}) for P_3 1.544–1.780, P_{21} 0.203–0.269 and P_{38} 0.100–0.138. Resulting CRE ages are T_3 2.2–2.5 Myr, T_{21} 5.2–7.0 Myr and T_{38} 4.4–6.9 Myr.
Interestingly, the model (Leya and Masarik, 2009) predicts $^{21}Ne/^{22}Ne$ ratios < 0.8 for many shielding conditions for the bulk chemistry of NWA 7034, because it is particularly sodium-rich, without the need to postulate the presence of solar cosmic ray- (SCR)-derived neon (see discussion by Krietsch (2020) and Wieler et al. (2016)). A ratio of ≤0.8 is considered there a good indicator for the presence of SCR-Ne.
The measured $^{36}Ar/^{38}Ar$ ratio has been decomposed into trapped and cosmogenic argon components, assuming $(^{36}Ar/^{38}Ar)_c$ is in the range 0.63–0.67 (Wieler et al., 2016) and $(^{36}Ar/^{38}Ar)_t$ in NWA 8114 ranges from air (5.319) to martian atmosphere (4.2 ± 0.1, (Atreya et al., 2013)).

Table 2
Summary of xenon data for the three NWA 8114 samples analysed using the RELAX mass spectrometer; full data tables with isotope ratios from individual heating steps are given in Table S2. The measured xenon isotope ratios can be modelled as a mixture of martian atmosphere, spallation and fission (with a contribution from terrestrial atmosphere in the first heating step of each sample): the concentrations of each component are given here as $^{132}Xe_{MA}$, $^{126}Xe_S$ and $^{136}Xe_F$ respectively.

Sample	Type	Mass (mg)	Max $^{129}Xe/^{132}Xe$[a]	Total ^{132}Xe ($\times 10^{-11}$ cm^3 STP g^{-1})	$^{132}Xe_{MA}$ ($\times 10^{-11}$ cm^3 STP g^{-1})[b]	$^{129}Xe_{excess}$ ($\times 10^{-11}$ cm^3 STP g^{-1})[c]	$^{126}Xe_S$ ($\times 10^{-12}$ cm^3 STP g^{-1})[b]	$^{136}Xe_F$ ($\times 10^{-12}$ cm^3 STP g^{-1})[b]
NWA8114_6a_1	Chip	2.56	2.423 (88)	1.84 (1)	1.29 (2)	2.08 (2)	1.16 (3)	1.28 (8)
NWA8114_6a_2	Chip	1.52	2.450 (45)	2.72 (2)	2.17 (3)	3.46 (3)	1.38 (4)	1.6 (1)
NWA8114_133	Matrix cuttings	1.33	2.288 (52)	2.45 (2)	1.76 (2)	2.71 (3)	1.23 (4)	1.5 (1)

Uncertainties are 1 σ, and are given in the units of the last decimal place.
[a] Maximum $^{129}Xe/^{132}Xe$ ratios are determined following a spallation correction, assuming a $^{129}Xe/^{126}Xe$ ratio of 1.6 ± 0.4 for both barium and REE spallation (Hohenberg et al., 1981). Figure 5 illustrates the effect of using $^{129}Xe/^{126}Xe$ ratios of 1 and 2.2 for the spallation correction, which raise and lower the maximum corrected $^{129}Xe/^{132}Xe$ ratios respectively, but values are within uncertainty of those quoted here.
[b] $^{132}Xe_{MA}$, $^{126}Xe_S$ and $^{136}Xe_F$ have been determined on the basis that most heating steps can be adequately modelled as a mixture of martian atmosphere, barium spallation, and a fission component derived from a mixture of ^{244}Pu and ^{238}U. Low temperature heating step for each samples require a contribution from terrestrial air. Three high temperature releases require a contribution from REE spallation for an acceptable fit.
[c] The concentration of excess ^{129}Xe is calculated over a solar $^{129}Xe/^{132}Xe$ ratio of 1.

In general, the gas extracted from each heating step was modelled adequately (i.e. χ^2 per degree of freedom < 2) as a mixture of martian atmosphere, barium spallation, and a spontaneous fission component (Table S3). Low temperature releases from each aliquot required a contribution from either terrestrial air or martian interior xenon; given that this is released at low temperature the most likely explanation is the presence of xenon adsorbed from the terrestrial atmosphere (e.g. Schwenzer et al., 2012). In addition, three high temperature releases require a contribution from spallation of light rare earth elements for an acceptable fit of the modelled isotopic composition to the experimental data. Acceptable models can be found for each release when either ^{244}Pu or ^{238}U is included as the sole fission parent, though χ^2 per degree of freedom is generally higher when uranium is chosen. The step heating data are thus consistent with the bulk analysis described above. All the individual releases can be accounted for without the need for an ancient martian atmospheric signature. These data are discussed further in Section 4.3.2, where Fig. 3 to Fig. 5 combine to support the models of the data: the plots show that no releases require an ancient atmospheric component.

4. Discussion

NWA 8114 is a breccia similar in terms of lithology and mineral content to the other NWA 7034 grouped stones (Supplementary Information Section S3.1); the noble gas composition and content is also broadly similar. These stones are uniquely placed to provide us with new information about Mars' ancient regolith surface, and how that surface and the rocks it contains has interacted with the martian atmosphere through time.

Ar-Ar ages of our sample of NWA 8114 (1.385 ± 0.021 Ga, Section S3.2) are similar to the age of 1.13–1.25 Ga determined for clasts in a different portion of NWA 8114 (MacArthur et al., 2019), and those for paired stones that range between ~ 1.191 and 1.391 Ga for whole rock fragments (Cassata et al., 2018; Lindsay et al., 2021). The span of Ar-Ar ages of plagioclase and feldspar separates is larger, from ~ 0.788 to 2.250 Ga (Lindsay et al., 2021). Other dating systems, including U-Pb ages of apatite (1.35–1.85 Ga; Bellucci et al., 2015; Hu et al., 2019; McCubbin et al., 2016; Yin et al., 2014) and lower-intercept discordant U-Pb ages on zircon (1.4–1.7 Ga; Bellucci et al., 2015; Hu et al., 2019; Humayun et al., 2013; McCubbin et al., 2016; Nemchin et al., 2014; Yin et al., 2014), also yield ages that are variable. It has been suggested that these differences in ages may reflect heterogenous resetting due to a prolonged and varied series of events, including metamorphic events (Cassata et al., 2018).

The halogen concentrations (Section S3.4 and Table S9) of the bulk NWA 8114 sample are high relative to other reported measurements for martian meteorites (e.g., Cartwright et al., 2013; Cartwright et al., 2014; Clay et al., 2020; Dreibus and Wänke, 1987) (Fig. S10). The Br/Cl ratio of NWA 8114 is broadly chondritic but the I/Cl is elevated compared to the chondritic value reported by Clay et al. (2017). The high concentration of iodine (1.9–2.8 ppm, compared to ~ 3 ppb to 1.7 ppm iodine in other martian meteorites) may suggest a component of terrestrial iodine contamination. Alternatively, the high iodine may derive from a halogen-rich phase like chlorapatite which is present in 2.2 % modal abundance in NWA 8114 (Fig. S4, Table S5). Iodine concentrations in chlorapatite from paired stone NWA 7533 are abundant but variable, ranging from 2 to 84 ppm (Bellucci et al., 2017).

4.1. Cosmic Ray Exposure Age

The measured cosmogenic "shielding indicator" $^{21}Ne/^{22}Ne$ (Table 1) indicates a low contribution from neutron capture on mainly ^{24}Mg compared to production from spallation, and so a relatively low secondary neutron flux. In addition, our modelling of the step heating xenon data using the approach of Crow et al. (2020) allowed the $^{131}Xe/^{126}Xe$ ratio associated with barium spallation to be calculated (Table S3). The correlation between the modelled contribution to ^{126}Xe from Ba spallation and excess ^{131}Xe calculated over the modelled composition (MSWD = 0.76) yielded $^{131}Xe/^{126}Xe$ = 3.56 ± 0.17. This calculation is based on the releases where a contribution from light rare earth element spallation was not required to achieve an acceptable fit, where ^{129}Xe was not included in the calculation of χ^2 to avoid assuming an underlying $^{129}Xe/^{132}Xe$ ratio in the martian atmospheric component, and where both U and Pu were allowed as potentially contributing to any fission component. $^{131}Xe/^{126}Xe$ ratios determined from similar calculations that allow just ^{244}Pu or just ^{238}U are within uncertainty of this value. The derived $^{131}Xe/^{126}Xe$ ratio indicates slightly lower production by secondary neutron capture on ^{130}Ba than observed by Hohenberg et al. (1981) in the angrite Angra Dos Reis ($^{131}Xe/^{126}Xe$ = 4.36 ± 0.11), and so is consistent with the conclusion based on neon isotopes.

For the determination of the cosmic ray exposure (CRE) age, we followed the method described by Wieler et al. (2016) and Krietsch (2020), to enable comparison with their large datasets comprising in total more than 50 recently found shergottites. These studies (see notes under Table 1) use a chemistry-dependent physical model (Leya and Masarik, 2009, and updates). Adopting the bulk chemistry of paired NWA 7034 (Agee et al., 2013) and the measured cosmogenic "shielding indicator" $^{21}Ne/^{22}Ne$ (Table 1); the

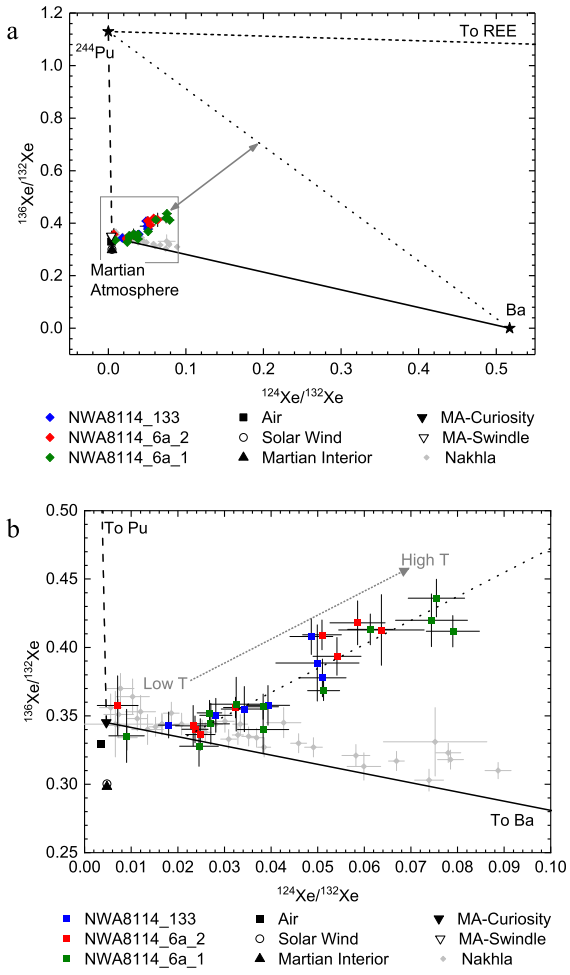

Fig. 3. (a) An overview graph of ^{136}Xe/^{132}Xe vs ^{124}Xe/^{132}Xe suggests data are consistent with mixing between two components. One of these components has a composition close to the modern martian atmosphere, with a low ^{124}Xe/^{132}Xe (and high ^{129}Xe/^{132}Xe) ratio. The other component has higher ^{136}Xe/^{132}Xe and ^{124}Xe/^{132}-Xe ratios (and a lower ^{129}Xe/^{132}Xe ratio), consistent with an intimate mixture of fission (here shown as ^{244}Pu) and spallation (Ba) xenon. The arrowed region indicates possible end members of the spallation-fission component mixed with the atmospheric component. On an expanded scale (b) the data indicate a small contribution of ^{124}Xe to the atmospheric component and two points with a low spallation contribution. If the lowest heating steps are excluded, the data show a linear trend of increasing ^{124}Xe/^{132}Xe and ^{136}Xe/^{132}Xe, as illustrated by the dotted black line. Both the fission and spallation contributions increase with increasing temperature, as shown by the grey arrow that indicates the general trend with increasing temperature. In a plot of ^{129}Xe/^{132}Xe vs ^{124}Xe/^{132}Xe (Fig. 4) it is apparent that these two (low temperature points) have a contribution from the terrestrial atmosphere. Literature values are shown for terrestrial atmospheric (air, (Basford et al., 1973)), solar wind (Crowther and Gilmour, 2013), martian atmosphere (MA) as measured by Curiosity (Conrad et al., 2016)) and in shergottite glasses (Swindle et al., 1986), martian interior (Mathew and Marti, 2001), ^{244}Pu fission (Ozima and Podosek, 2002) and Ba and REE spallation (Hohenberg et al., 1981) components. Ratios are derived from data in Table S2, and data points with large uncertainties (^{129}Xe/^{132}Xe and ^{136}Xe/^{132}Xe errors greater than 5 % of the measured values) are excluded for clarity and scale. Data for Nakhla (Gilmour et al., 2001) are shown as small light grey diamonds for comparison.

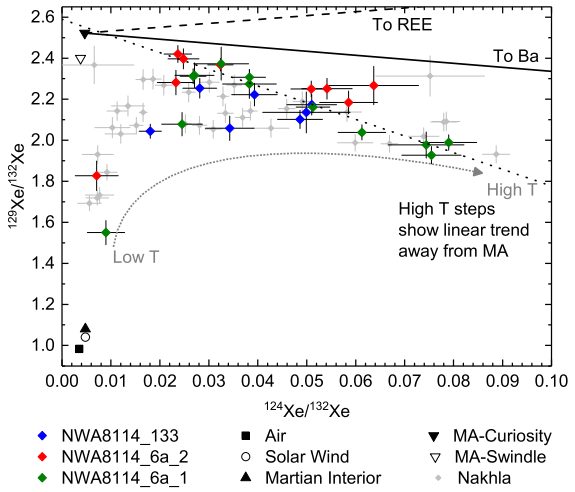

Fig. 4. The ^{129}Xe/^{132}Xe vs ^{124}Xe/^{132}Xe ratios show fission mixing with spallation. The lowest temperature heating steps have the lowest spallation contributions, i.e. ^{124}Xe/^{132}Xe ratios closest to the martian atmosphere ratio. These steps also include a small amount of contamination from the terrestrial atmosphere. As the temperature increases, the spallation contribution increases, increasing the ^{124}Xe/^{132}Xe ratio, as indicated by the grey arrow. The heating steps with the highest spallation contributions (highest ^{124}Xe/^{132}Xe ratios) are also those with the highest fission contributions (lowest ^{129}Xe/^{132}Xe ratios), suggesting the fission component is associated with the spallation component. If the lowest heating steps are excluded, the data show a linear trend away from the martian atmosphere composition, as illustrated by the dotted black line. Literature values for end members and data for Nakhla are the same as in Fig. 3.

model examines a range of potential pre-atmospheric meteoroid sizes and considers 4π irradiation. In this case the model suggests that the low relative contribution of ^{21}Ne from neutron capture is most likely achieved in a pre-atmospheric meteoroid radius of 20 cm – larger radius meteoroids exhibit significantly higher secondary neutron fluxes at all exposure positions. Production of ^{80,82}Kr from neutron capture on bromine isotopes requires a radius at least 30–55 cm (Marti et al., 1966), suggesting the observed excesses of ^{80}Kr and ^{82}Kr may have been produced in the martian regolith rather than during the meteoroid's transit from Mars.

Using the production rate ranges for cosmogenic ^{21}Ne and ^{38}Ar (see notes under Table 1) we calculate T_{21} ages in the range 5.2–7.0 Myr and T_{38} ages in the range 4.4–6.9 Myr. From these we estimate the CRE age to be 5.7 ± 1.3 Myr (see Table 1 for details). This is consistent with most of the many CRE ages covering a large range determined for NWA 7034, NWA 7906 and NWA 7907 (Cartwright et al., 2014; Stephenson et al., 2017; Cassata et al., 2018) and hence supports the suggestion, based mostly on chemistry and petrology, that NWA 8114 is paired with these stones (Section 1.2). As these stones are known to be derived from the same strewnfield, they will have experienced the same Mars to Earth transit history, and any differences may be due to different burial depths in the original meteoroid, and/or different exposure histories on the surface of Mars.

Differences in the ages are likely due to the distinct methods used to calculate production rates and heterogeneity in target element chemistry. Our age production rate takes account of the very high concentration of sodium and low concentration of magnesium in NWA 7034 and its pairs. Cartwright et al. (2014) favour a ^{3}He and ^{38}Ar$_c$ age of ~ 5 Myr, based on production rates by Eugster and Michel (1995), over their ^{21}Ne$_c$-derived CRE age of ~ 9 Myr. They preferred a pre-atmospheric radius of 50 cm, determined using the model by Leya and Masarik (2009), with a radius of 10–25 cm, consistent with the radius determined here, being also possible. In contrast, Cassata et al. (2018) gave apparent ages between 2 Myr (^{3}He) and 12 Myr (^{78}Kr), with their ^{21}Ne and ^{38}Ar ages being intermediate, at 4 to 5 Myr. These ages have also been calculated with the production rate scheme by Eugster and Michel (1995) which also covers cosmogenic krypton and xenon isotopes, and a nominal shielding of 40 g/cm^2, i.e. ~ 14 cm shielding.

Due to the use of distinct models and differently derived shielding conditions, CRE ages are not easy to compare, and the concentrations of ^{3}He, ^{21}Ne and ^{38}Ar (Table 1) might be more useful. The

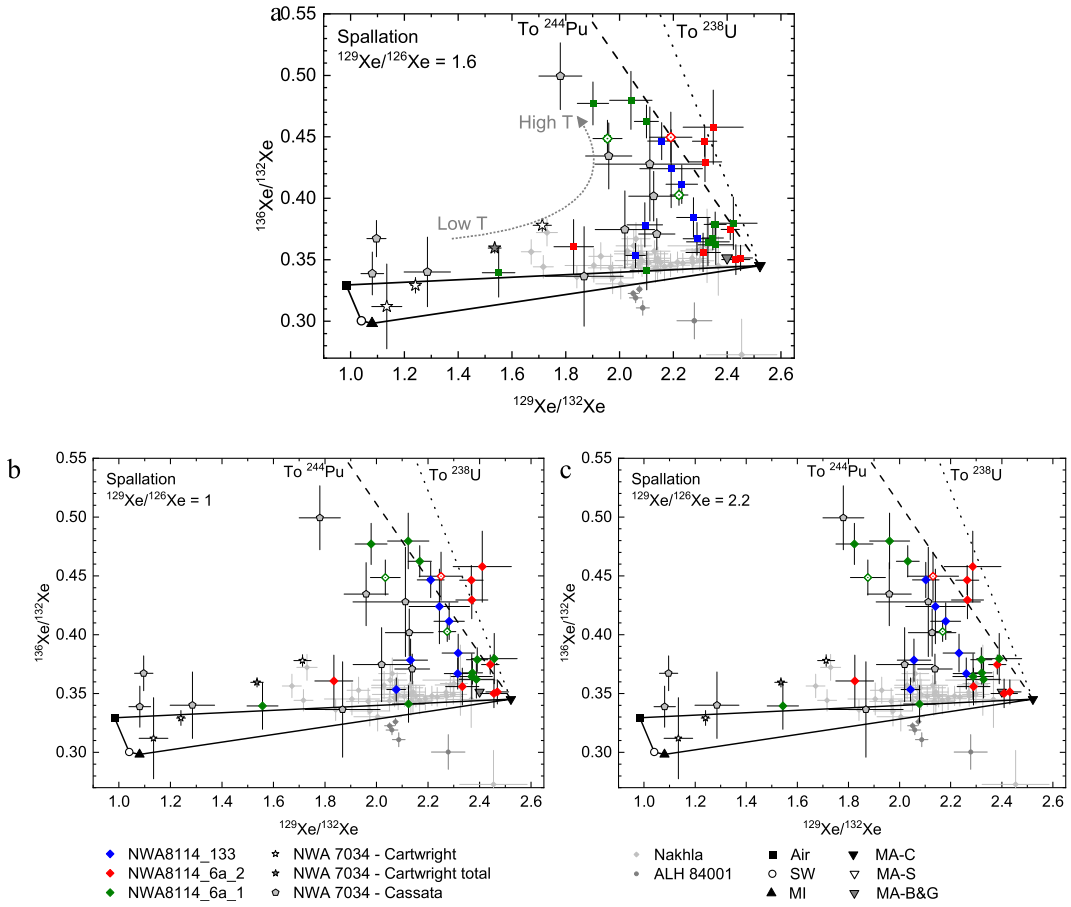

Fig. 5. Mixing diagram of $^{136}Xe/^{132}Xe$ vs $^{129}Xe/^{132}Xe$ for data that have been corrected for a spallation contribution. (a) Data corrected using the $^{129}Xe/^{126}Xe$ ratio of 1.6 ± 0.4 adopted for both barium and REE spallation by Hohenberg et al. (1981). The steps which required a contribution from REE spallation are shown as open diamonds with a dot in the centre, in the same colours as the other heating steps for that sample (one heating step for the sample labelled NWA8114_6a_2, and two heating steps for that labelled NWA8114_6a_1). Several steps have $^{129}Xe/^{132}Xe$ ratios consistent with the modern martian atmosphere. Many steps have high $^{136}Xe/^{132}Xe$ ratios, indicative of a contribution from spontaneous fission of ^{244}Pu and/or ^{238}U: the data might suggest that the fission component in NWA8114_133 and NWA8114 _6a_1 (blue and green points) is dominated by ^{244}Pu, and that in NWA8114_6a_2 (red points) by ^{238}U, but it is not possible to conclusively identify one source and eliminate the other from these data. As the temperature increases, so too does the fission contribution; the grey arrow indicates the general trend with increasing temperature. The data are also corrected using $^{129}Xe/^{126}Xe$ ratios of 1 (b) or 2.2 (c) for the spallation component, to illustrate that different ratios can be obtained for the underlying martian atmosphere component, depending on the choice of $^{129}Xe/^{126}Xe$ ratio for the spallation component. Data for NWA 7034 are also shown (Cartwright et al., 2014; Cassata, 2017), and have been corrected for spallation contributions as detailed in the original publications. Literature values for end members and data for Nakhla are the same as in Fig. 3. Selected data for ALH 84001 (Swindle et al., 1995; Gilmour et al., 1998; Mathew and Marti, 2001), which illustrate the lower $^{129}Xe/^{132}Xe$ and $^{136}Xe/^{132}Xe$ ratios of the ancient martian atmosphere compared to the present day values, are also shown.

lowest and highest concentrations of the helium, neon and argon isotopes (Cartwright et al., 2014; Cassata et al., 2018; this work) vary unsystematically. The concentrations measured in NWA 7034 by Cartwright et al. (2014) and Cassata et al. (2018) (only their *average* concentrations) are mostly within < 30 % of those measured here for NWA 8114. Only ^{3}He given by Cartwright et al. (2014) is more than a factor of two higher than those given by Cassata et al. (2018) and here. The noble gas concentrations could, hence, broadly be taken to support the suggestion based mostly on chemistry and petrology, that NWA 8114 is paired with NWA 7034 (Section 1.2). In detail, the measured gas concentrations show enormous variations, likely reflecting that the NWA 7034 rocks are brecciated and even the major element chemistry can vary significantly at the 10s of mg scale. In spite of this, our ^{3}He CRE age of ~ 2.3 Myr is similar to the ^{3}He age of Cassata et al. (2018) and much lower than the ages determined for ^{21}Ne and ^{38}Ar. The ^{3}He age determined by Cartwright et al. (2014) in contrast is close to their preferred ~ 5 Myr. This illustrates that the same production rate systematics need to be used before age distributions for martian meteorites (and other meteorites) can be rigorously compared.

4.2. U-Xe Age

As discussed in Section 3.2, the xenon isotopic signature includes a fission component, although it is not possible to distinguish from the measured isotope ratios whether this is from spontaneous fission of ^{244}Pu, spontaneous fission of ^{238}U, or a mixture of the two. A bulk uranium concentration has not been measured for NWA 8114, but a concentration of 0.512 ± 0.024 ppm is reported for NWA 7034 (Agee et al., 2013), and 0.29 ± 0.03 ppm for NWA 7475 (Wittmann et al., 2015). Based on the concentration of fission-derived xenon in the samples and these uranium concentrations, it is possible to calculate apparent U-Xe ages (Table 3 and supplementary Section S3.3). It should be noted that this group of meteorites are heterogeneous, and the bulk uranium concentrations are not necessarily representative of the uranium concentrations of the small amounts of material (<2.6 mg) analysed in this study. The calculated ages using these bulk concentrations must, therefore, be evaluated with that in mind.

The U-Xe ages calculated using the NWA 7034 bulk uranium concentration do not exceed the age of the sample so there is no requirement for an additional ^{244}Pu contribution, but that does

Table 3
U-Xe and Pu-U-Xe ages calculated from bulk uranium concentrations reported for NWA 7034 (Agee et al., 2013) and NWA 7475 (Wittmann et al., 2015), and estimated uranium concentrations for these samples.

Sample	U-Xe Age (Ga)[a]			Pu-U-Xe Age (Ga)[b]	
	NWA 7034 bulk U	NWA 7475 bulk U	Estimated U[c]	NWA 7475 bulk U	Estimated U[c]
NWA8114_6a_1	3.06 ± 0.20	4.70 ± 0.41	4.77 ± 0.25	4.02 ± 0.4	4.03 ± 0.4
NWA8114_6a_2	3.68 ± 0.27	5.54 ± 0.50	4.99 ± 0.31	4.11 ± 0.3	4.06 ± 0.4
NWA8114_133	3.46 ± 0.26	5.24 ± 0.48	5.22 ± 0.33	4.09 ± 0.3	4.08 ± 0.3

[a] U-Xe ages are calculated from $^{136}Xe_F$ concentrations (Table 2), assuming the fission component is entirely derived from ^{238}U, and assuming $\lambda_{sf}^{136}Y_{sf}$ to be 6.83×10^{-18} a^{-1} (Ragettli et al., 1994).
[b] Calculations of Pu-U-Xe ages also incorporate an initial Solar System Pu/U ratio of 0.0068 ± 0.0010 (Hudson et al., 1989), along with a ^{244}Pu branching ratio of 1.25×10^{-3} and ^{136}Xe yield of 5.6 % (Ozima and Podosek, 2002).
[c] See Supplementary information Section S3.3 for further information about the estimated uranium concentrations.

not necessarily rule it out; we revisit this in the next section. In contrast, the ages calculated from the NWA 7475 bulk uranium concentration are older than the sample and therefore require a contribution from ^{244}Pu (Table 3). We also estimate uranium concentrations for the individual samples (Section S3.3), which are very similar to the concentration in NWA 7475. Again, the ages calculated from these concentrations are older than the sample and require a ^{244}Pu contribution.

In situ production of ^{244}Pu fission Xe would require formation more than 4 Gyr ago; a Sm-Nd internal isochron yielded an age of 4.39 Ga (Nyquist et al., 2016), and old U-Pb ages (~4.4 Ga) have been reported for zircons in NWA 7034 and NWA 7533 (Humayun et al., 2013; Nemchin et al., 2014). Zircon grains have been identified in the NWA 8114 sample (Section S3.1, Table S5, Fig. S3d, Fig. S4, Fig. S7j), so this is a realistic proposition. If the ^{244}Pu fission component was produced *in situ*, Pu-U-Xe ages for these samples are ~ 4 Ga (Table 3). However, parentless ^{244}Pu fission xenon has previously been identified in martian meteorites (Mathew and Marti, 2001, 2002; Ocker and Gilmour, 2004), and, if an inherited component is present in the meteorites analysed here, then the fission signature would preserve no chronological information.

4.3. Ancient or Modern Martian Atmosphere in NWA 8114?

4.3.1. Krypton and Xenon Elemental Abundances

Data from our krypton and xenon elemental analyses are similar to those from analysis of both Nakhla (Mathew and Marti, 2002) and ALH 84001 (Mathew and Marti, 2001), in that the $^{84}Kr/^{132}Xe$ ratios lie to the left of mixing lines between the martian interior and the modern martian atmosphere (Fig. 2b). In the case of Nakhla, this has been interpreted to be a consequence of elemental fractionation of a noble gas component derived from the martian atmosphere before or during incorporation into the host rock (Ott, 1988; Drake et al., 1994). So, while it remains possible that this represents a change in the elemental composition of the martian atmosphere over time (e.g., Cassata, 2017; Mathew and Marti, 2001), we suggest that elemental fractionation favouring the heavy elements is the norm during incorporation of noble gases into a solid phase from an ambient atmosphere, and it is the Shergottite impact melt glass samples that are exceptional in this respect, in that their noble gases were shock implanted without mass fractionation (Bogard et al., 1986). For meteorites that are finds rather than falls, it has been shown that incorporation of noble gases from the Earth's atmosphere during terrestrial surface weathering leads to elemental fractionation favouring the heavy elements (Scherer et al., 1994; Schwenzer et al., 2013). The extent of this fractionation is very similar in martian meteorites found in both hot and cold deserts, suggesting differences in temperature and moisture on Earth do not lead to major differences in fractionation (Mohapatra et al., 2009; Schwenzer et al., 2013). Therefore, a similar process might be expected to operate on Mars in spite of the different ambient temperature and moisture, leading to fractionation of the martian atmospheric noble gas signatures in martian meteorites (Schwenzer et al., 2013). The identification of calcium carbonate on the martian surface indicates that weathering processes did, indeed, operate on Mars in the past (Boynton et al., 2009; Bultel et al., 2019). And the presence of calcium carbonate (calcite) in our sample of NWA 8114 (Table S5, Figs. S3 and S8) implies that it experienced weathering processes at some point in its history. Aqueous alteration on Mars has also been proposed (e.g., Drake et al., 1994) to play a role in this fractionation; alteration similar to that which has affected Nakhla has been reported in paired meteorites of NWA 8114/7034 (Table S6 and MacArthur et al., 2019). Thus, noble gas element abundances do not require the presence of a contribution from the ancient martian atmosphere.

4.3.2. Xenon Isotopic Data

Each of our individual temperature release steps are consistent with the elevated $^{129}Xe/^{132}Xe$ ratio being derived from the modern martian atmosphere, so we now consider mixing diagrams to examine whether trends in the data provide further constraints. In Fig. 3 and Fig. 4 we show that our data from NWA 8114 resemble Nakhla data previously reported. Gilmour et al. (2001) acquired data from Nakhla samples that had been lightly etched with acid, washed in water, and left untreated (two replicates of each). We restrict discussion here to the releases from samples that had been water-washed or acid-etched, as these treatments resulted in removal of most terrestrial atmospheric xenon (Gilmour et al., 2001). They reported that data exhibited mixing between two end-members; one with small or no contribution from spallation xenon and an elevated $^{129}Xe/^{132}Xe$ ratio of 2.350 ± 0.026, and one consisting of a mixture of martian interior xenon and spallation that was reproducible within the precision of the data. In step heating experiments, the former component (i.e. that with a high $^{129}Xe/^{132}$-Xe ratio) was released before the latter, with a clear contribution from the terrestrial atmosphere at the lowest temperatures (Fig. 4). This release pattern, terrestrial air at the lowest temperatures, followed by a high $^{129}Xe/^{132}Xe$ component, and then increasing contributions from a spallation-rich signature at higher temperature, is similar to that observed in NWA 8114 (see Fig. 4).

Fig. 3 relates the $^{124}Xe/^{132}Xe$ and $^{136}Xe/^{132}Xe$ ratios, illustrating mixing between one or more trapped components (candidate sources are modern martian atmosphere, ancient martian atmosphere, terrestrial air and martian interior), spallation, and fission end members (see Fig. caption for references). (As noted above, spallation is dominated by production from barium, while it is not possible in any release to unambiguously identify whether the fission parent is ^{238}U or ^{244}Pu). In both Nakhla and NWA 8114, $^{124}Xe/^{132}Xe$ increases with release temperature, indicating an increasing proportion of spallation xenon. In Fig. 3, Nakhla data

indicate a mixture between martian atmosphere and a spallation component, whereas NWA 8114 data require a significant contribution from a fission component that appears to be well mixed with spallation xenon. Barium and uranium are both large, incompatible atoms. Barium is primarily hosted in K-feldspars, and uranium in chlorapatite, both of which are present in NWA 8114 (Table S5) and paired stones (Humayun et al., 2013). Although the abundance of chlorapatite is low (~2 %, Table S5), it is highly enriched in uranium and may be the source of the fission xenon component. However, phosphates are also the primary host of REE, so it is perhaps somewhat surprising that there is little evidence of REE spallation in the xenon isotopic signature. Without further analyses of mineral separates, we can only speculate about the host phases of these xenon components. The principal constraint from Fig. 3 is that the Ba-spallation component and the U-fission component are present in rather uniform ratios within each of the temperature steps. Since no single mineral host is known to have both elements in sufficient abundances, the abundant fine-grained lithologies including the intraclast matrix and the clast-laden melt rocks (CLMR, (Hewins et al., 2017); see also Wittmann et al., 2015; McCubbin et al., 2016) are likely petrologic features corresponding to the sources of both Xe components.

Fig. 4 relates the $^{124}Xe/^{132}Xe$ and $^{129}Xe/^{132}Xe$ ratios. It is apparent that low temperature releases include a component with a low $^{129}Xe/^{132}Xe$ ratio that is most readily interpreted as terrestrial air ($^{129}Xe/^{132}Xe$ = 0.9832, (Basford et al., 1973)), mixed with a trapped component. The trapped component is close in composition to the modern martian atmosphere ($^{129}Xe/^{132}Xe$ = 2.5221 ± 0.0063, (Conrad et al., 2016)), with a high $^{129}Xe/^{132}Xe$ ratio.

Considering Fig. 3 and Fig. 4 together, apart from the lowest temperature releases, data from both Nakhla and NWA 8114 are consistent with mixing between a component with low $^{124}Xe/^{132}Xe$ and a second component with high $^{124}Xe/^{132}Xe$. In Fig. 3 NWA 8114 data form a linear trend that intersects with the mixing line from modern martian atmosphere to Ba spallation, suggesting that a small contribution from spallation is present alongside martian atmospheric xenon in NWA 8114. Plausible petrologic features corresponding to the sources of this trapped atmospheric component accompanied by Ba-spallation are the vitrophyres that contain veins with Ba-rich feldspar (Hewins et al., 2017). In Fig. 4, both Nakhla and NWA 8114 data require that the spallation-rich endmember include a contribution of ^{132}Xe from other sources. In Fig. 3, elevated $^{136}Xe/^{132}Xe$ ratios indicate that in the case of NWA 8114 this includes a fission contribution. In the case of Nakhla, it may be martian interior xenon, though Mathew and Marti (2002) identified a contribution from Pu fission xenon as well.

From these mixing diagrams we conclude that the additional component alongside spallation in NWA 8114 is fission xenon (Fig. 3). The decomposition of individual releases detailed in Section 3.2 supports this conclusion: the gas extracted in individual heating steps was modelled as a mixture of martian atmosphere, barium spallation, and a fission component. In Nakhla a similar data analysis demonstrates there is a contribution from martian interior xenon alongside the spallation component, as originally proposed by Gilmour et al. (2001).

In Fig. 4, the step releases with the lowest spallation contribution that lie on the mixing line (i.e., contain no clear contribution from terrestrial air) have $^{124}Xe/^{132}Xe \approx 0.02$. We now explore the effects of a spallation correction to the data. The $^{129}Xe/^{126}Xe$ ratio from spallation of both Ba and REE elements is not well constrained; Hohenberg et al. (1981) adopted 1.6 ± 0.4 for both targets. Because the uncertainty in the ratio introduces a systematic error affecting all data in the same sense, we show the effects of assuming $^{129}Xe/^{132}Xe$ = 1.6, 1.0 and 2.2 in Fig. 5, illustrating that different ratios can be obtained for the underlying martian atmosphere component depending on the choice of the $^{129}Xe/^{126}Xe$ ratio used for the spallation correction. As noted above, acceptable fits of modelled compositions to each individual release can be found when either ^{244}Pu or ^{238}U is included as the sole fission parent. However in Fig. 5 the data fall into groups corresponding to the separate sample aliquots, suggesting that the fission components in the samples labelled NWA8114_133 and NWA8114_6a_1 are dominated by ^{244}Pu, whereas that in NWA8114_6a_2 is dominated by ^{238}U. This difference between aliquots is not a surprising result given the diversity of clast types and mineral compositions seen within the NWA 8114 main mass (Supplementary Movie 1) and section (Figs. S3 and S4, Tables S2 and S3). Ancient zircon crystals have been identified in paired stones NWA 7034 and NWA 7533 (Humayun et al., 2013; Nemchin et al., 2014) that could, in principle, have incorporated live ^{244}Pu and retained its fission products, but other zircons show evidence of disturbance after ^{244}Pu was extinct (Yin et al., 2014), which may have resulted in degassing of ^{244}Pu-derived xenon. Once again, these mixing diagrams demonstrate that xenon from our NWA 8114 samples is entirely consistent with high $^{129}Xe/^{132}Xe$ ratios being caused by a contribution from the modern martian atmosphere. The highest measured $^{129}Xe/^{132}Xe$ ratios are ~ 2.4 (Table S2). This places a lower limit on the "true" composition of the martian atmospheric component: it could, in principle, have a higher $^{129}Xe/^{132}Xe$ ratio if the measured value is mixed with another component, but atmospheric ratio cannot be lower than the measured value.

To determine numerical constraints on the $^{129}Xe/^{132}Xe$ and $^{136}Xe/^{132}Xe$ ratios of the underlying spallation- and fission- free component in NWA 8114 and Nakhla we return to Fig. 3 and Fig. 4. In both NWA 8114 and Nakhla, the measured point least affected by spallation xenon and terrestrial air has $^{124}Xe/^{132}Xe \approx 0.02$. (Only the very lowest temperature heating steps have $^{124}Xe/^{132}Xe$ ratios lower than ~ 0.02, and these are consistent with air contamination.) In the case of NWA 8114 data points with $^{124}Xe/^{132}Xe \approx 0.02$ may represent the endmember: a component derived from the martian atmosphere mixed with pure spallation; the composition of this component lies at the intersection of the trend line from the data with the mixing line between modern martian atmosphere and barium spallation in Fig. 3. Although it might appear that the trend line could extend to a composition closer to the solar composition (Fig. 3), there are no data points below the mixing line between the modern martian atmosphere and barium spallation, i.e. no analyses with low $^{136}Xe/^{132}Xe$ ratios characteristic of the ancient martian atmosphere. The measured $^{136}Xe/^{132}Xe$ ratio of this endmember is thus consistent with the modern martian atmosphere. The corresponding $^{129}Xe/^{132}Xe$ ratio is obtained by making a spallation correction to the point on the trendline established by the data at $^{124}Xe/^{132}Xe$ = 0.02; this yields $^{129}Xe/^{132}Xe$ = 2.46 ± 0.03, which is within 2 σ of the modern martian atmospheric value 2.5221 ± 0.0063 (Conrad et al., 2016). Thus the trends in the data can be accounted for by modern martian atmosphere contributing the xenon responsible for the elevated $^{129}Xe/^{132}Xe$ ratio.

Alternatively, the trend lines defined by the data can be extrapolated to the point where $^{124}Xe/^{132}Xe$ = 0.00464 (Fig. 4). This leads to $^{129}Xe/^{132}Xe$ = 2.55 ± 0.03 for NWA 8114 (identical within error to the modern martian atmosphere). However, $^{136}Xe/^{132}Xe$ is then 0.305 ± 0.008, significantly lower than the martian atmosphere ratio of 0.3452 ± 0.0022 (Conrad et al., 2016). While this might be an expected composition of an ancient martian atmospheric signature, as noted in the previous paragraph there are no data on the trend line that require its presence. Similar extrapolations for the other xenon isotopes give ratios that are, for the most part, within 2 σ of the modern atmospheric values; the only other exception is $^{134}Xe/^{132}Xe$ ratio which is also slightly low, but there are again no data points with low $^{134}Xe/^{132}Xe$ ratios. The majority of isotopes point towards a modern atmospheric composition.

The xenon isotopic plots should not be taken in isolation from each other, they must be considered together to fully understand and properly interpret the data. If the trend lines in Fig. 3 and Fig. 4 were to be extrapolated to a $^{136}Xe/^{132}Xe$ ratio of ~ 0.3, then a line through the data in Fig. 5 would also have to be extrapolated to the same value. This would give a $^{129}Xe/^{132}Xe$ ratio higher than that of the modern martian atmosphere, whereas the ancient atmosphere is characterised by a lower $^{129}Xe/^{132}Xe$ ratio.

In the case of Nakhla, extrapolation of the trend line yields $^{129}Xe/^{132}Xe = 2.34 \pm 0.03$, while making a spallation correction to the composition on the line where $^{124}Xe/^{132}Xe = 0.02$ leads to $^{129}Xe/^{132}Xe = 2.30 \pm 0.02$. Each interpretation yields a $^{129}Xe/^{132}Xe$ ratio for the Nakhla component lower than that of the present day martian atmosphere by more than 5 σ.

We thus find no compelling evidence for 'ancient' martian atmospheric xenon in our analyses of NWA 8114. Instead we suggest that the previous identification (Cassata, 2017) was either an unfortunate coincidence resulting from consistent releases of a mixed component, or a consequence of sample heterogeneity – our data cannot rule out the possibility that other portions (stones) or different lithologies of this regolith breccia definitively record an ancient atmosphere isotopic signature, but there is no compelling evidence for its presence in the material we have investigated. The ancient zircon crystals identified in NWA 7034 and NWA 7533 (Humayun et al., 2013; Nemchin et al., 2014) demonstrate that there are components in these meteorites that are, in principle, old enough to have incorporated an ancient atmospheric component, but the range of resetting events dated by the Ar-Ar age of NWA 8114 and several other chronometers (Section 1.2) indicate that any ancient component experienced subsequent thermal resetting that could have partially or totally erased the ancient noble gas component (e.g., Lindsay et al., 2021). If the estimated U-Xe ages (Section 4.2) are chronologically significant, they suggest that some phases (likely zircon) retained a significant fraction of xenon produced by *in situ* decay of ^{238}U and ^{244}Pu over their history, but the martian atmosphere component was incorporated more recently.

The low $^{129}Xe/^{132}Xe$ ratio observed in Nakhla is, however, intriguing since it appears to be sampled by all the high temperature releases from the four aliquots reported by Gilmour et al. (2001). At the time of publication this appeared to be consistent with modern martian atmospheric xenon (as determined from Shergottite glass (Mathew et al., 1998; Swindle et al., 1986)). In light of the Curiosity datum (Conrad et al., 2016), with its higher $^{129}Xe/^{132}Xe$ ratio, it is worthy of re-examination. It appears that there are two possible explanations; it represents a consistent mix of martian interior xenon with martian atmospheric xenon, or it samples a martian atmosphere trapped since the formation of Nakhla 1.38 Gyr ago (Nyquist et al., 2001) that had, at that point, not evolved to the present day $^{129}Xe/^{132}Xe$ ratio. We consider that a reproducible mixture of interior and atmospheric xenon is hard to envisage in a surface-correlated component (the atmospheric component in Nakhla is associated with acid leachable iodine (Gilmour et al., 2001), Section 1.1). The Ar-Ar isochron age of NWA 8114 (1385 ± 21 Ma, Fig. S 9a) is identical to the crystallisation age of Nakhla, but the different $^{129}Xe/^{132}Xe$ ratios observed in the two meteorites suggests that they sampled the martian atmosphere at different times. NWA 8114 sampled the atmosphere recently, when the $^{129}Xe/^{132}Xe$ ratio had evolved to the present-day value. In the next section we develop a model to understand the implications of the presence of spallation xenon in the martian atmosphere and consider further constraints that might be imposed if Nakhla records an earlier stage in its xenon isotopic evolution.

4.4. Evolution of the Martian Atmosphere, 3.7 Gyr to the present

The history of the martian atmosphere can be broadly divided into two periods: the first period was characterised by a high carbon dioxide pressure and possibly a greenhouse effect, the second by a low pressure generally similar to the environment today (e.g., Fanale et al., 1992). The transition between the two may have been initiated by polar condensation of carbon dioxide, ~3.7 Gyr ago (e.g., Gierasch and Toon, 1973; Haberle et al., 1994; Jakosky and Jones, 1997; Pepin, 1994).

The modern martian atmosphere xenon isotopic composition suggests an underlying primordial composition inherited from the early solar system that was modified by mass fractionation and acquired ^{129}Xe from the decay of ^{129}I (Conrad et al., 2016). Depending on the choice of the underlying starting composition (solar wind, U-Xe, chondritic xenon) a small contribution from fission (most likely of ^{244}Pu) may also be present in the modern atmosphere (Swindle and Jones, 1997; Pepin, 2000; Conrad et al., 2016). The components observed in martian meteorites indicate contributions from other reservoirs that must correspond to regions of the martian crust/mantle (e.g. the martian interior component incorporated in Chassigny, which is distinct from the martian atmosphere (Mathew and Marti, 2001)). These reservoirs include a source of solar xenon and a reservoir with a high relative abundance of xenon from fission of ^{244}Pu. In addition, the present-day composition of the martian atmosphere requires that a reservoir enriched in ^{129}Xe from ^{129}I was at least formerly present, but as yet a distinct source of that reservoir has not been definitively identified in the sample suite. Evolution from the base composition to the atmospheric composition observed today can be inferred to have taken place over Mars' geological history, with a general expectation that the atmosphere became more radiogenic over time as daughter isotopes were released from reservoirs that preferentially incorporated their parent elements.

Assuming that the present day atmosphere persisted for the last 3.7 Gyr, Conrad et al. (2016) calculated that 43 % of ^{80}Kr generated in the regolith from secondary neutrons over that time is in the present day atmosphere. They assume that the 43 % degassing also applies to xenon derived from barium spallation in the regolith. To explore the possibility that the $^{129}Xe/^{132}Xe$ ratio has evolved in the last 1.38 Gyr (i.e., since the crystallisation of Nakhla (Nyquist et al., 2001)) we have developed a simple model of martian atmospheric evolution within the same time frame. Since the two endmembers we identify in Nakhla are identical within 1 σ error, we adopt $^{129}Xe/^{132}Xe = 2.33 \pm 0.05$ for this component (to incorporate the upper and lower limits of the two values calculated in Section 4.3.2).

The specifics of the model are discussed in the following sections; in summary, we consider the evolution of the martian atmosphere following collapse of the early atmosphere. The amount of ^{132}Xe present acts as a proxy for the thickness of the atmosphere, which is assumed to be uniform and not vary with altitude. It is assumed that ^{132}Xe is lost from the atmosphere in the same proportion as other species, i.e. the fraction of ^{132}Xe in the atmosphere remains constant; however later we discuss the effects of relaxing this constraint. Excess ^{129}Xe, produced from decay of ^{129}I in the crust before the start of the model, is degassed into the atmosphere, causing the $^{129}Xe/^{132}Xe$ ratio to increase over time. Cosmic ray interactions with barium and rare earth elements in the regolith produce spallation derived xenon isotopes, which are also degassed into the atmosphere. The model aims to reproduce the $^{129}Xe/^{132}Xe$ ratios recorded by ALH 84001 and Nakhla at the times the signatures were trapped in those meteorites, the present day $^{129}Xe/^{132}Xe$ ratio as measured by the Curiosity rover (Conrad et al., 2016), and the fraction of spallation derived xenon in the

present day atmosphere calculated by Conrad et al. (2016). This is achieved by varying the atmospheric loss rates and crustal/regolith outgassing rates. Although there are several individual heating steps in our analyses of NWA 8114 that are identical within uncertainty to the modern martian atmosphere (Fig. 5), we choose to use the xenon composition of the modern (i.e., present day) atmosphere determined by the Curiosity rover (Conrad et al., 2016) in this model because it is more precise than our values. Furthermore, our data, or indeed data from other meteorites, are complicated by additional components (e.g. fission). Atmospheric loss has two consequences for the model. If the atmosphere was thicker in the past, production rates of spallation xenon in the regolith were lower due to reduced penetration of secondary cosmic-rays. Furthermore, some of the spallation xenon degassed from the regolith will be lost along with the other constituents of the atmosphere. This sets a limit on the extent of atmospheric loss allowed within the model. This simple model assumes a single phase of atmospheric collapse, but there may have been several such events, e.g. caused by giant impacts.

4.4.1. Characteristics of the Model

As a starting point, it is assumed there are two distinct periods in the evolution of Mars' atmosphere (Section 4.4); our model considers only the second phase. During the first period extensive degassing drove development of a dense atmosphere, which elevated the $^{129}Xe/^{132}Xe$ ratio from an initial solar composition to the value observed in ALH 84001 $\sim$ 4 Gyr ago (Gilmour et al., 1998). It is assumed that the atmosphere was too thick to allow any significant production of spallation xenon in the crust during this period. The second period occurred after atmospheric collapse more recently than 3.7 Gyr ago; our model tracks the evolution of the xenon signature over this interval. The less dense atmosphere now allows for production of spallation xenon in the crust, and degassing of both spallation xenon and ^{129}Xe make notable contributions of the xenon isotopic composition of the atmosphere. Any low-level degassing of the atmosphere during this period is considered to have occurred by different processes from the early degassing phase.

Within the timeframe considered by the model, it is assumed that the original atmosphere persisted up to a time of atmospheric collapse (τ_c – model parameters are defined in Table 4). Thereafter, the atmospheric xenon was modified by: (1) loss of xenon either from the atmosphere to space, or possibly by mineral/clathrate sequestration at the surface; (2) crustal outgassing of ^{129}I-derived ^{129}Xe (hereafter $^{129}Xe^*$), and (3) outgassing of spallation xenon from the upper $\sim$ 5 m of the regolith (i.e., the zone interacting with cosmic rays (Rao et al., 2002)). Both (1) and (2) occurred at a rate much lower than during formation of the pre-collapse atmosphere; and (3) is assumed negligible until after the collapse event occurred because the thick atmosphere prevented production of cosmogenic xenon in the regolith. The $^{129}Xe/^{132}Xe$ ratio at the time of atmosphere collapse is assumed to be that measured in ALH 84001 (1.95 ± 0.18 (Gilmour et al., 1998)), where the $^{129}Xe^*/^{132}Xe$ ratio (the ratio of excess ^{129}Xe to ^{132}Xe) is 0.95. Following collapse, further low-level loss of atmospheric xenon is recorded by the ^{132}Xe content of the atmosphere. Because the production of ^{132}Xe in the regolith is insignificant, the abundance of this isotope declines exponentially post-collapse with a mean life t_a (in each exponential decay term, the mean life is the reciprocal of the decay constant) in the model. It is assumed that the same proportion of the atmospheric budget of each xenon isotope is lost in any time step. By assuming a constant volume fraction of ^{132}Xe in the atmosphere (i.e. ^{132}Xe is lost from the atmosphere in proportion to other atmospheric species), the mass of the atmosphere immediately after collapse is set by the mean life of ^{132}Xe loss post-collapse and the present day abundance of ^{132}Xe. (The effect of relaxing this constraint is discussed below.).

The low $^{136}Xe/^{132}Xe$ ratio of xenon in ALH 84001 relative to the modern atmosphere suggests that the atmosphere was fractionated in favour of the heavy isotopes since its trapping in ALH 84001. The ALH 84001 datum at $\sim$ 4 Ga may record a pre-collapse atmospheric xenon signature and collapse may therefore have played a role in causing the fractionation observed in the modern atmosphere; conversely, it may record the xenon isotopic composition after atmospheric collapse which would imply the fractionation also occurred after collapse. However, we adopt the $^{129}Xe/^{132}Xe$ ratio recorded by ALH 84001 as the starting point of our model and do not include mass fractionation.

It is assumed that, before the start of the model, ^{129}I was sequestered into a crustal reservoir with negligible xenon and with

Table 4
Summary of $^{129}Xe/^{132}Xe$ ratios and parameters used in the model for the evolution of the martian atmosphere (Section 4.4). A mean lifetime t_x is the reciprocal of the decay constant for the corresponding process, λ_x.

$^{129}Xe/^{132}Xe$ ratios		
Source	$^{129}Xe/^{132}Xe$	Time
ALH 84001	1.95 ± 0.18	Adopted at atmosphere collapse, post crystallisation at ~4.5 Ga (Gilmour et al., 1998; Nyquist et al., 2001)
Nakhla	2.33 ± 0.05	Post crystallisation at 1.38 Ga (Gilmour et al., 2001; Nyquist et al., 2001)
Curiosity	2.5221 ± 0.0063	Present day (Conrad et al., 2016)

Spallation	
Target	
43 %	Of spallation produced in crust in the baseline model with no atmospheric loss, is in present day atmosphere (Conrad et al., 2016)

Model parameters		
Parameter	Description	Input or Calc[a]
τ_c	Time of collapse of original high mass atmosphere	Input
t_a	Mean life of (post collapse) atmospheric degassing Dictates the thickness of the atmosphere at the start of the model	Input
t_l	Mean lifetime of outgassing of $^{129}Xe^*$ from the crust into the atmosphere	Calc
t_d	Mean lifetime of regolith processing, i.e. of outgassing of spallation xenon from the crust into the atmosphere	Calc

[a] Indicates whether each parameter is an input value for the model, or whether it is calculated (Calc) as an output from the model.

negligible sources of other xenon isotopes. In particular, we follow previous workers (e.g., Musselwhite and Drake, 2000) by noting that the martian atmosphere has a large excess from ^{129}I decay but little or no evidence of excesses of isotopes produced by fission of ^{244}Pu, requiring that iodine and plutonium were geochemically or otherwise separated into distinct reservoirs early in the history of Mars. We assume that, in the period covered by the model, ^{129}Xe* was degassed from this reservoir to the atmosphere with a rate declining exponentially with mean life t_I. Three observed ^{129}Xe/^{132}Xe ratios help to constrain the degassing of ^{129}Xe*: the initial ^{129}Xe/^{132}Xe ratio of the martian atmosphere at the start of the model is stipulated by the ALH 84001 ratio (Gilmour et al., 1998); the ^{129}Xe/^{132}Xe ratio observed in Nakhla (Gilmour et al., 2001) provides a snapshot of the composition of the atmosphere at the time it was incorporated into the meteorite; and the value measured by the Curiosity Rover (Conrad et al., 2016) corresponds to the present day composition.

We also assume that processing of the regolith (that leads to degassing of spallation xenon) declined exponentially with a mean life t_a. Assuming the current atmospheric conditions and the current cosmic ray flux prevailed for at least the last 3.7 Ga, and taking a plausible concentration of bromine in the regolith, Conrad et al. (2016) showed that 43 % of the ^{80}Kr generated in the regolith by secondary neutrons over the last 3.7 Gyr currently resides in the atmosphere. They assume the 43 % regolith degassing also applies to spallogenic xenon products. Our model is constructed to duplicate this result rather than explicitly parameterising target element concentration and cosmic ray flux. That is to say, the production rate at the present day is chosen so that, with a constant atmospheric pressure over the lifetime of the model, 43 % of the total production of spallation xenon would be present in the atmosphere today. To account for the lower production of spallation xenon under a thicker atmosphere, we assume that the production rate at the surface varies purely as a function of the thickness of the overlying atmosphere.

When atmospheric loss is allowed during the period considered by the model (i.e. low level loss after collapse), the earlier, thicker atmosphere at the start of the model lowers the production rate of spallation xenon from the modern baseline. To address this, the data of Hohenberg et al. (1978) are used to model the effects of an increased atmospheric mass. For shielding depths greater than 20 g cm^{-2} the data are consistent with a production rate that is an exponentially decreasing function of shielding depth with a mean depth of 136 g cm^{-2} (an average between those for production from barium and light rare earth elements: 154 and 118 g cm^{-2} respectively).

4.4.2. Implications for Martian history since 3.7 Ga

For the baseline model (τ_c = 3.7 Ga, with no further loss of xenon from the atmosphere after collapse) a constant degassing rate of 0.034 % Myr^{-1} of the regolith budget of spallation-produced xenon is sufficient to account for the spallation content of the modern martian atmosphere. This degassing rate is independent of the production rate of spallation xenon, as the target is 43 % of the spallation xenon produced over 3.7 Gyr is in the present day atmosphere rather than an absolute concentration. If a higher or lower proportion is required in the atmosphere, the degassing rate must increase or decrease respectively. The production and degassing rates can, however, be used to determine an absolute amount of spallation xenon in the atmosphere in this baseline model. The model can then be varied to reproduce this amount of spallation xenon under different conditions. Fig. 6a, for example, plots the accumulation of spallation xenon in the atmosphere as a function of time for different atmosphere thicknesses at the start of the model, aiming to reproduce the same absolute amount of spallation xenon in the present day atmosphere.

If xenon loss is permitted after collapse, but with a very long mean lifetime t_a (i.e., when the mass of the atmosphere has been effectively constant since collapse), atmospheric collapse can have occurred no more recently than τ_c = 1.7 Ga. At this point the spallation xenon content of the atmosphere today (as determined by the baseline model) is equal to the total generated in the regolith since atmospheric collapse.

If atmospheric loss over time is allowed (post collapse), the total spallation xenon that must be degassed to account for the present-day abundance increases, because some of the degassed spallation xenon has been lost over time. However, atmospheric loss necessitates a thicker initial (post collapse) atmosphere than today, reducing the production rate of spallation xenon isotopes (Fig. 7a and b). Together these constraints imply that more spallation xenon must be produced, however the production rate has increased with time, imposing a limit on the maximum initial atmospheric mass at the start of the model and the loss history. In models where the atmosphere collapsed at τ_c = 3.7 Ga, in order to accumulate sufficient spallation derived xenon in the present-day atmosphere and satisfy the conditions imposed by the ^{129}Xe/^{132}Xe ratios (discussed below), the atmosphere at the start of the model was no more than 4.9 times more massive than today's, with a loss rate of 0.043 % Myr^{-1} (Fig. 7b). A thicker initial (post-collapse) atmosphere and associated faster loss rate does not allow for a sufficient amount of spallation xenon to accumulate in the atmosphere (Fig. 6). For more recent τ_c the maximum allowable loss rate decreases, and, therefore, the atmospheric mass at τ_c is lower in order to accommodate the lower loss rate over the shorter time period involved.

In the baseline model it is assumed that the xenon signature of Nakhla records the atmospheric composition at its crystallization age of 1.38 Ga (Nyquist et al., 2001), and the ^{129}Xe/^{132}Xe ratio is one of the target ratios the model uses to calculate the mean lifetime for ^{129}Xe* outgassing (t_I). Since the atmospheric ^{132}Xe content is constant in this baseline model (i.e. no loss after collapse), the rate of change of the observed ^{129}Xe/^{132}Xe ratio between trapping in Nakhla (at 1.38 Ga) and the present day is similar to that between 3.7 Ga, when the ^{129}Xe/^{132}Xe ratio was that recorded by ALH 84001, and the time of trapping in Nakhla (Fig. 6b). For this reason, the mean lifetime for degassing of ^{129}Xe* into the atmosphere, t_I, is very long (10.7 Gyr - in effect the degassing rate of ^{129}Xe* can be considered constant). Models that allow for atmospheric loss require higher rates of ^{129}Xe* degassing early on (Fig. 7a and b), and so shorter t_I values (because larger amounts of ^{129}Xe* degassed early on in the model have been lost more effectively, Fig. 6c). Later collapse times also require shorter t_I values: it is assumed that degassing of ^{129}Xe* before collapse was not sufficient to affect the ^{129}Xe/^{132}Xe ratio of the prevailing, thick atmosphere, so later collapse allows less time to evolve from the ALH 84001 ratio to that of Nakhla, while the time available to evolve from the Nakhla value to the present day remains the same (Fig. 6d). Conversely, for declining rates of degassing of ^{129}Xe* to the atmosphere, as might be expected based on the decline in volcanic activity, atmospheric loss after collapse is required to account for the Nakhla datum.

Gilmour et al. (2001) speculated that the atmospheric signature in Nakhla may have been incorporated by shock rather than at crystallisation, possibly due to the event that ejected it from the martian surface. If the time of trapping of the atmospheric signature in Nakhla is more recent than the crystallization age there is an increased need for atmospheric loss, i.e., an increased need for the atmosphere at the start of the model to be thicker than the present day. This is because later trapping of the Nakhla signature means the ^{129}Xe/^{132}Xe ratio has less time to evolve between the Nakhla and present day values, requiring a higher degassing rate of ^{129}Xe* into the atmosphere. This, in turn, would have rapidly

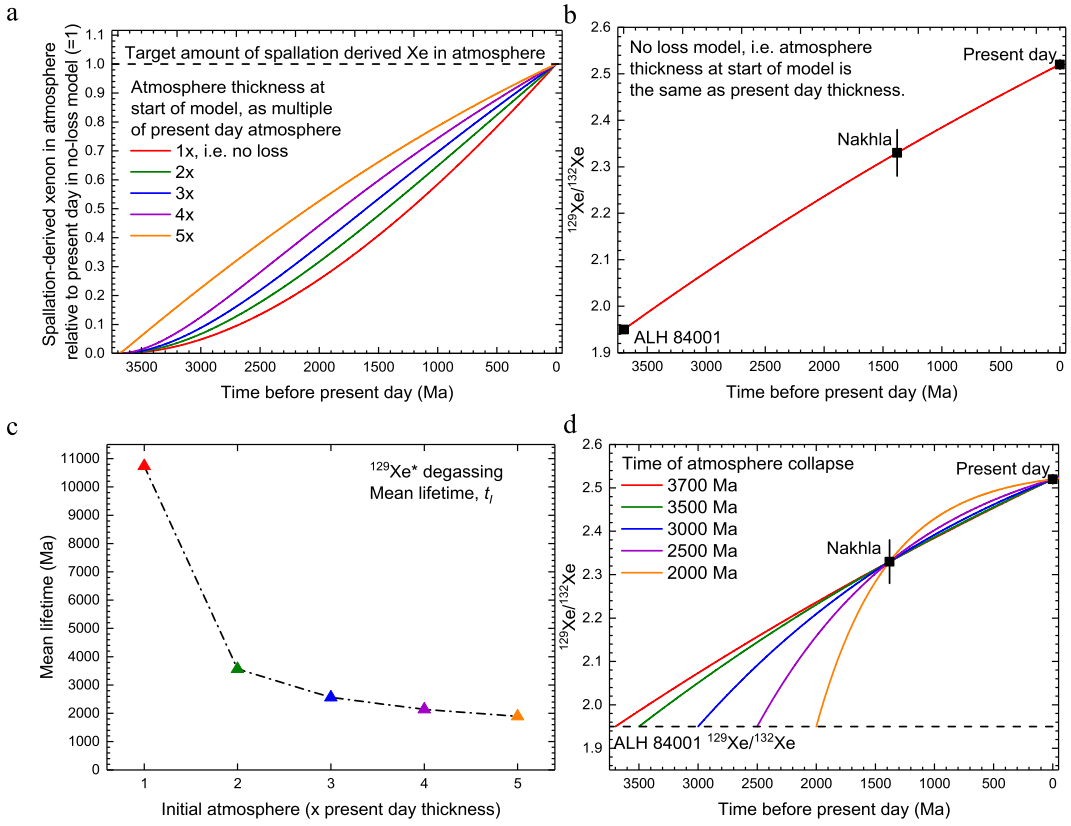

Fig. 6. Illustrations of the model for the evolution of the martian atmosphere discussed in Section 4.4.2. (a) shows the amount of spallation derived xenon in the atmosphere as a function of time. Assuming there is no further loss from the atmosphere after collapse 3.7 Gyr ago (i.e. the thickness of the atmosphere 3.7 Gyr ago was the same as the present day thickness), the baseline model targets 43 % of the spallation xenon produced in the crust over the last 3.7 Gyr being in the present day atmosphere (Conrad et al., 2016). If the atmosphere 3.7 Gyr ago was thicker than the present day, the model aims to reproduce the same absolute final amount of spallation xenon in the present day atmosphere, and examples for an initial atmosphere between twice and five times the density of the present day atmosphere are illustrated. However the denser initial atmosphere reduces the production of spallation xenon, and necessitates atmospheric loss. (b) illustrates the $^{129}Xe/^{132}Xe$ ratio as a function of time, again assuming there was no further loss from the atmosphere after collapse 3.7 Gyr ago. The $^{129}Xe/^{132}Xe$ ratio at the start of the model is assumed to be 1.95 as recorded in ALH 84001 (Gilmour et al., 1998) and the Nakhla signature is assumed to have been trapped when the rock crystallised at 1.38 Ga (Nyquist et al., 2001). The rate of change of the $^{129}Xe/^{132}Xe$ ratio between trapping in Nakhla and the present day is similar to that between the start of the model at 3.7 Ga and the time of trapping in Nakhla. Models for initial atmospheres between twice and 5 times the present day thickness produce almost identical curves to that shown in (b), but require higher $^{129}Xe^*$ outgassing rates early on, and hence shorter $^{129}Xe^*$ lifetimes, t_l, as illustrated in (c). (d) shows the effect of later atmospheric collapse on the evolution of the $^{129}Xe/^{132}Xe$ ratio as a function of time, assuming no further atmospheric loss for a range of collapse times between 3.7 and 2.0 Ga. It is assumed that the $^{129}Xe/^{132}Xe$ ratio recorded in ALH 84001 represents the ratio at the time of collapse, and therefore later collapse allows less time to evolve from the ALH 84001 ratio to the Nakhla ratio, while the time to evolve from the Nakhla value to the present day ratio is unchanged, requiring shorter mean lifetimes for the outgassing of $^{129}Xe^*$ from the crust into the atmosphere, t_l. If collapse occurred more recently than ~ 2 Ga and there was no further loss, it is not possible to reproduce the ALH 84001, Nakhla and present day $^{129}Xe/^{132}Xe$ ratios in this no-loss scenario.

driven up the ratio between 3.7 Ga and trapping in Nakhla unless the atmosphere was thicker during this period.

The constraint imposed by the cosmic ray spallation signature observed in the modern martian atmosphere (i.e. in order for sufficient spallation xenon to accumulate in the atmosphere, the initial post-collapse atmosphere at 3.7 Ga can have been no thicker than 4.9 times the present day, with an atmospheric loss rate no greater than 0.043 % Myr^{-1}) requires that the Nakhla datum be recorded no more recently than 720 Myr ago, for consistency with a $^{129}Xe^*$ degassing rate that is constant or declining over time. It is hard to avoid these constraints on initial atmospheric mass and time of trapping in Nakhla since it is the loss of spallation-derived xenon from the atmosphere that plays the largest role in providing this constraint, rather than the reduced production rate caused by the early, thicker atmosphere. The model age of possible atmospheric trapping significantly predates the ejection of Nakhla from Mars (estimated to have occurred ~ 11 Ma ago (Nyquist et al., 2001)). A shock event that affected the nakhlites has also been identified at 630 Ma (Daly et al., 2019). If the xenon was incorporated by this earlier shock event, it would require later collapse of the early atmosphere accompanied by atmospheric loss through the duration of the model, for consistency with both a declining $^{129}Xe^*$ degassing rate and the amount of spallation derived xenon in the present day atmosphere.

Our model tracks the ^{132}Xe content of the atmosphere, and up to this point, we have assumed other chemical species are lost from the atmosphere in the same proportion as ^{132}Xe (Fig. 7a and b). Xenon should be the least likely species to escape from a planetary atmosphere by Jeans escape, but it is highly depleted relative to the other noble gases in the terrestrial atmosphere and, to a lesser extent, the martian atmosphere (e.g., Ozima and Podosek, 2002; Zahnle, 1993). Whereas loss of xenon may have occurred preferentially in an early thick atmosphere (e.g., Avice and Marty, 2020; Zahnle et al., 2019), once the bulk of the atmosphere is gone, the same xenon loss process probably does not operate and xenon may then switch to being the least efficiently lost (Scherf and Lammer, 2020). It is possible to see the effects of allowing differential loss of xenon by decoupling the production rate of spallation in the regolith (dependent on total atmosphere) from the amount of ^{132}Xe in the atmosphere. If xenon was lost less efficiently from the atmosphere compared with other species, the initial atmosphere must have been thicker than implied by the initial xenon

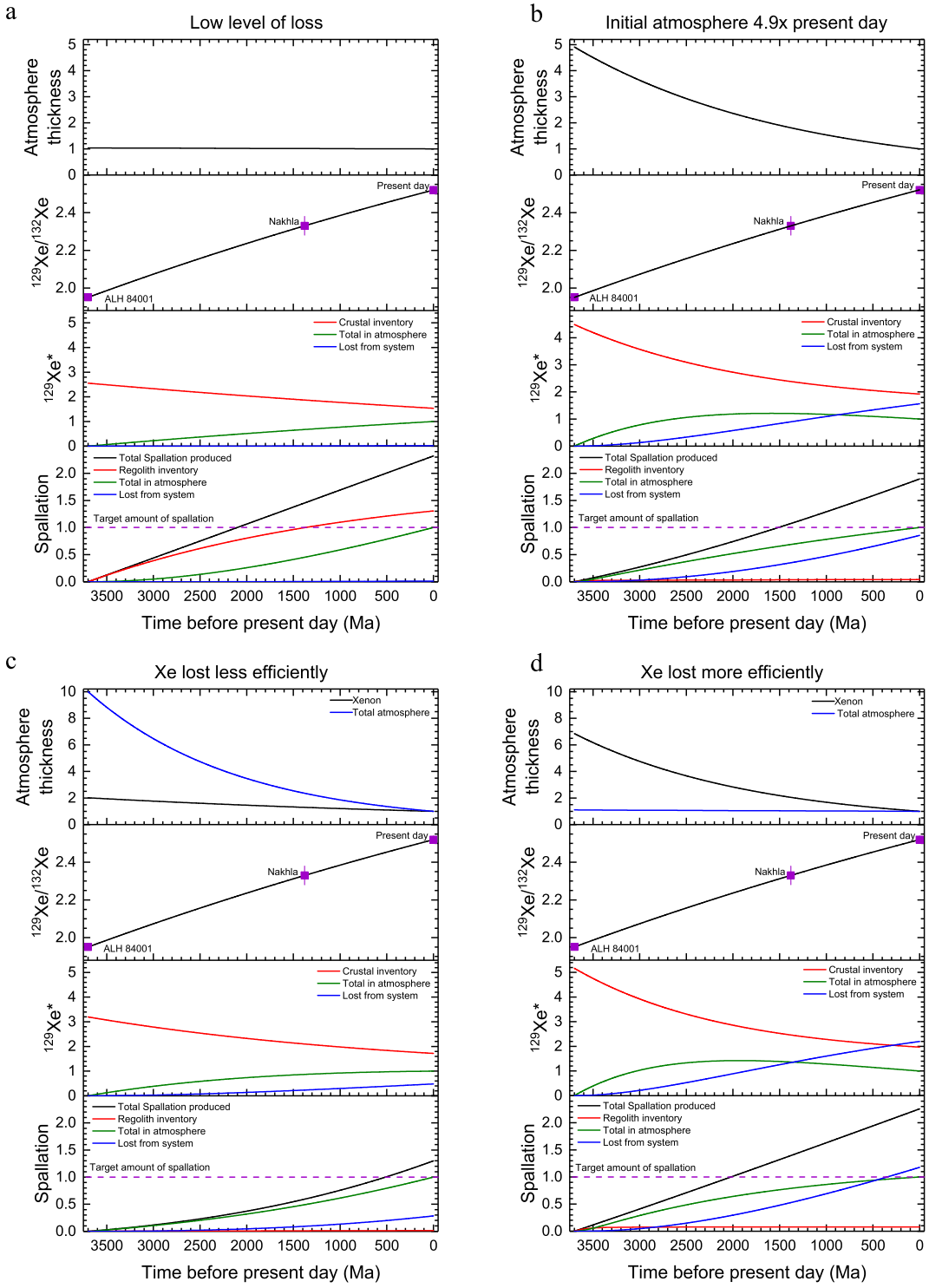

Fig. 7. Each stack of graphs illustrates how the atmosphere thickness, $^{129}Xe/^{132}Xe$ ratio, amount of ^{129}Xe and amount of spallation vary with time, for a different scenario in the model of the evolution of the martian atmosphere. The top plot in each stack illustrates the thickness of the atmosphere relative to the present day atmosphere (=1); the second shows the evolution of $^{129}Xe/^{132}Xe$ ratio, with ratios recorded in ALH 84001, Nakhla and the present day ratio also shown; the third plot show the crustal inventory of $^{129}Xe^*$, the amount in the atmosphere, and the amount lost from the atmosphere, relative to the amount of $^{129}Xe^*$ in the present day atmosphere in the baseline, no-loss model (=1); and the bottom plot in each stack shows the total amount of spallation xenon produced, and how much of that remains in the regolith, is in the atmosphere, and has been lost, again relative to the target amount of spallation in the present day atmosphere in the no-loss model (=1). (a) illustrates these quantities in a model with a very long mean lifetime and associated low level of loss; (b) shows an initial atmosphere 4.9 times more massive than the present day atmosphere. (c) considers a scenario where xenon was lost from the atmosphere less efficiently than other species, with an example in which the mass of the initial atmosphere was 10 times higher than today, in which case the initial xenon mass can only have been ~ 2.0 times higher than today. (d) considers a scenario where xenon was lost more efficiently than other species, using an example where the initial atmosphere was only 10 % higher than today, and the initial xenon mass can have been no more than 6.8 times higher than today. Note the scale of the thickness of the atmosphere (top plot) in (c) and (d) is different to that in (a) and (b).

abundance. Therefore, the initial spallation production in the regolith would have been lower than that assumed from the xenon abundance. For example, if the mass of the atmosphere was 10 times higher than today at the start of the model, the xenon mass can only have been 2 times higher than today (Fig. 7c). Combined with a reduction in the production of spallation-derived xenon in the regolith due to the thicker atmosphere, a higher loss rate associated with a higher initial xenon mass would prevent sufficient spallation xenon accumulating in the atmosphere. Similarly, if we consider a hypothetical situation where xenon was lost more efficiently from the atmosphere than other species, the initial atmosphere was not as thick as implied by the xenon abundance, and the initial spallation production would have been correspondingly higher. For example, if the mass of the atmosphere at the start of the model was only 10 % higher than today, the xenon mass can have been no more than 7 times higher than today (Fig. 7d). Although, in this case, ample spallation-derived xenon is produced in the regolith, a higher initial xenon mass and associated higher loss rate, again, does not allow sufficient spallation xenon to accumulate in the atmosphere.

Volcanic activity on Mars has declined over time (Greeley and Spudis, 1981; Carr and Head, 2010), and so magmatically driven degassing of $^{129}Xe^*$ might also be expected to have decreased over time. Higher, early degassing rates require atmospheric loss to account for the change in $^{129}Xe/^{132}Xe$ ratios from ALH 84001, to the Nakhla value, then to the present day value. When the requirement for a constant volume fraction of xenon in the atmosphere is relaxed (i.e. when the model hypothetically allows for xenon to be lost from the atmosphere more or less efficiently than other species), higher initial atmospheric masses reduce the scope for loss of xenon. This is because there is less production of spallation xenon in the regolith, the total amount of spallation xenon produced is lower, and so less xenon can be lost in the model. Because there is less scope for loss of xenon over time, the rate at which $^{129}Xe^*$ is added to the atmosphere by degassing from the interior (λ_I) is lower. Thus, to have a decline in degassing rate for $^{129}Xe^*$, linked to a decline in volcanic activity, the volume fraction of ^{132}Xe in the atmosphere has to be higher at the start of the model than at the end, which means that xenon has to be lost more readily than the major constituents of the atmosphere. This is perhaps counterintuitive if the gases are lost to space, however it might be possible if the loss process is trapping on surfaces in a way that removes xenon from the atmosphere over the lifetime of the model. The heavier noble gases have stronger Van der Waals bonding than the lighter species, so are preferentially adsorbed on surfaces. Laboratory measurements using analogues for the martian regolith predict that at least 90 % of xenon could be adsorbed on the regolith, compared to up to 25 % of krypton (Fanale et al., 1978). In this case the xenon would be lost from the atmosphere to a surface reservoir more readily than other species, but not lost to space.

Observations of erosion rates, valley networks, and surface mineralogy on the martian surface indicate a transition to a low mass atmosphere around the time of the late heavy bombardment at $\sim$ 3.9 Ga (e.g., Bottke et al., 2015; Carr, 2012), while the rate of volcanic activity has declined over the period since (Greeley and Spudis, 1981; Carr and Head, 2010). Combined with the constraint on the $^{129}Xe/^{132}Xe$ ratio imposed by Nakhla, our model indicates that this requires loss of xenon from the martian atmosphere over the last 3.7 Gyr (i.e. since collapse of an initial, thick atmosphere) with the present day budget being as little as 20 % of that at the start of this period.

To summarise, our model investigates the presence of spallation xenon in the martian atmosphere, with the additional constraints imposed if the $^{129}Xe/^{132}Xe$ ratio observed in Nakhla records an earlier stage in the xenon isotopic evolution of the martian atmosphere when compared to the present day ratio. The baseline model assumes no further atmospheric loss after atmospheric collapse at 3.7 Ga, and 43 % of the spallation xenon produced in the crust since that time is in the present day atmosphere. If atmospheric loss is permitted over time, the thicker initial atmosphere reduced the production rate of spallation xenon, and requires that some of the degassed spallation xenon is lost over time, imposing a limit on the maximum initial thickness of the atmosphere. Combining the constraint on the $^{129}Xe/^{132}Xe$ ratio imposed by Nakhla with declining $^{129}Xe^*$ degassing rates, requires loss of xenon from the martian atmosphere over the last 3.7 Gyr (i.e. since collapse of an initial, early, thick atmosphere), and the present day budget is as little as 20 % of that at the start of this period.

4.5. Formation of Martian Volatile Reservoirs

Bulk silicate material accounts for 70 % of the mass of Mars, and the iodine concentration in bulk silicate Mars is estimated to be in the range 6 to 36 ppb (Taylor, 2013; Clay et al., 2020). But halogen abundances vary greatly in martian materials, covering 4–5 orders of magnitude (Clay et al., 2020 and references therein). The iodine concentration of NWA 8114 measured in this work is 1930 ± 140 ppb (Sections 3 and S3.4). Using the total mass and mean molecular weight of the martian atmosphere, along with the abundance of xenon (Mars Fact Sheet), we calculate that the modern atmosphere contains 7.8×10^{33} atoms $^{129}Xe^*$. If we adopt the upper and lower limits of the bulk silicate iodine concentration (as above), and assume that 50 % of the bulk silicate iodine took part in crust formation (similar to chlorine, (Taylor, 2013)) and subsequently degassed into the atmosphere, this requires an initial $^{129}I/^{127}I$ ratio in the range $\sim 1.2 \times 10^{-6}$ to $\sim 2 \times 10^{-7}$, corresponding to "closure" to $^{129}Xe^*$ loss around 100 to 150 Myr after solar system formation ($^{129}I/^{127}I = 10^{-4}$ (Brazzle et al., 1999)). Our models allow for a loss of 80 % of the atmospheric xenon budget present at 3.7 Ga, corresponding to a reduction in the closure interval of around two half-lives of ^{129}I ($\sim$72 to 110 Myr after solar system formation). This is at odds with the proposal that Mars is a remnant planetary embryo that completed its growth within the first 4 Myr of solar system history (Dauphas and Pourmand, 2011). For consistency, we would require that atmospheric collapse removed a fraction of xenon, or that a largely un-degassed interior reservoir has stored xenon produced by ^{129}I decay.

Under what circumstances can the volatile reservoirs inferred from martian meteorites form? These reservoirs include an atmosphere enriched in the decay product of ^{129}I, but lacking the decay product of ^{244}Pu, an interior reservoir with a solar xenon signature, and separate reservoirs dominated by decay products of ^{129}I and ^{244}Pu. The reservoir with a solar xenon signature requires that at least some of the martian interior was un-degassed, so that radiogenic decay did not significantly alter the primordially trapped xenon isotope signature. Solidification of a magma ocean (e.g., Elkins-Tanton, 2008; Lammer et al., 2013) provides a natural route to degas a substantial portion of a planet of its xenon, while creating separate reservoirs concentrating iodine and plutonium (Musselwhite and Drake, 2000). Xenon degassed as the crust formed must be lost from Mars before subsequent release of iodogenic $^{129}Xe^*$ can lead to the observed high $^{129}Xe/^{132}Xe$ ratio of the atmosphere. Early crust formation can produce a xenon reservoir dominated by $^{129}Xe^*$ even if plutonium and iodine are incorporated quantitatively. For instance, a reservoir formed at 20 Myr after solar system formation would have evolved to $^{136}Xe^*/^{129}Xe^* = 0.0010$ after a further 50 Myr of ^{244}Pu decay ($^{136}Xe^*$ denotes ^{136}Xe produced from spontaneous fission of ^{244}Pu) (Fig. S11). Such a reservoir can act as a source to enrich the $^{129}Xe^*$ of the martian atmosphere. After complete decay, this reservoir would reach

$^{136}Xe^*/^{129}Xe^*$ = 0.0026 (Fig. S11), allowing it to be a candidate source for the continued evolution of the martian atmosphere's $^{129}Xe/^{132}Xe$ ratio during the 3.7 Gyr period covered by our model without producing a measurable increase in the $^{136}Xe/^{132}Xe$ ratio.

However, at least some plutonium must be concentrated in a reservoir depleted in iodine to produce the observed fissiogenic interior component (Chass-E, Fig. 1). This requires that iodine and plutonium were at least partially separated during crust formation; the residue of the iodine-rich reservoir can then act as a source driving further atmospheric evolution while the plutonium-rich reservoir can act as a source of the parentless fission xenon identified in Chass-E. Such a model can account for the early formation of Mars in spite of its late apparent closure interval – a significant fraction of ^{129}Xe from ^{129}I decay is still trapped in a solid planetary reservoir.

The final reservoir required by Curiosity observations (Conrad et al., 2016) is dominated by spallation of barium and must be in the upper 5 m of the regolith (i.e., in the zone where cosmic-rays can penetrate). Assuming a 43 % degassing efficiency, Conrad et al. (2016) calculate that a regolith barium concentration of 602 ppm over a depth interval of $\sim$ 500 g/cm^2 is needed to account for the observed excesses of ^{124}Xe and ^{126}Xe in the atmosphere. If complete degassing is assumed, the concentration decreases to 300 ppm. This concentration is much higher than estimates for the martian crust (4.37 ppm (Taylor, 2013)) and bulk concentrations measured in other NWA 7034 grouped stones ($\sim$100–150 ppm (Humayun et al., 2013; Wittmann et al., 2015) where barium is likely hosted in K-feldspar (Table S5), hyalophane (Hewins et al., 2017) and evolved petrological rock types (Fig. S6)). However analyses by Sojourner, the MER rovers and Curiosity on the surface of Mars indicate a more evolved composition (summarised by Sautter et al. (2016)): measurements of barium using the Chemistry Camera ('ChemCam') instrument onboard the Curiosity Rover show local enrichments up to 1500–2000 ppm in individual pebbles and rocks (Ollila et al., 2014). A martian regolith barium concentration of 300 ppm is not excessive if terrestrial analogue systems are considered (e.g., Best, 2003; Li, 2000).

5. Conclusions

In this work we have analysed the noble gas composition of the martian meteorite NWA 8114. Helium, neon and argon show no evidence of a trapped composition; the measured ^{3}He, ^{21}Ne and ^{38}Ar appear to be entirely cosmogenic (Table 1). The heavy noble gases krypton and xenon are elementally fractionated with respect to the present day martian atmosphere and the terrestrial atmosphere, similar to Nakhla. Using production rates for cosmogenic ^{21}Ne and ^{38}Ar we estimate the CRE age to be 5.7 ± 1.3 Myr. CRE ages for paired stones cover a large range between $\sim$ 2 and 12 Ma (Cartwright et al., 2014; Stephenson et al., 2017; Cassata et al., 2018), and our age falls in the middle of this range. However, it is important to note that we used partly different methods to calculate production rates and target element chemistry than were used to calculate NWA 7034 CRE ages, and that in order to properly compare ages across these (and other) samples the same production rate systematics need to be used.

The xenon isotopic composition we measured in NWA 8114 shows evidence of a component enriched in ^{129}Xe (relative to a solar $^{129}Xe/^{132}Xe$ ratio of $\sim$ 1), a spallation component, and a fission component. The gas extracted in most heating steps can be adequately modelled as a mixture of the modern martian atmosphere, barium spallation, and a fission component (although it is not possible to distinguish whether the fission component is from ^{244}Pu, ^{238}U or a mixture of the two). Low temperature releases require a contribution of terrestrial air, and three high temperature releases require a contribution from spallation of rare earth elements. Data are consistent with two component mixing, between (i) a component close to the modern martian atmosphere (high $^{129}Xe/^{132}Xe$, low $^{136}Xe/^{132}Xe$), with a small contribution from spallation xenon, and (ii) an intimate mixture of fission and spallation xenon (low $^{129}Xe/^{132}Xe$, high $^{136}Xe/^{132}Xe$ and $^{124}Xe/^{132}Xe$). The maximum (spallation corrected) $^{129}Xe/^{132}Xe$ ratio observed is 2.4 50 ± 0.045 (Table 2), which is within 2σ uncertainty of the the Curiosity measurement (Conrad et al., 2016). We see no evidence of a contribution from the ancient martian atmosphere (characterised by a lower $^{129}Xe/^{132}Xe$ ratio of $\sim$ 1.95 to $\sim$ 2.17 (Gilmour et al., 1998; Mathew and Marti, 2001)) in these analyses.

We developed a model for the evolution of the martian atmosphere, to investigate the evolution of the $^{129}Xe/^{132}Xe$ ratio (recorded by ALH 84001, Nakhla and observed at the present day) and the amount of spallation xenon in the atmosphere. The baseline model assumes collapse of Mars' early atmosphere 3.7 Gyr ago (with no further loss of xenon after collapse), after which magmatic degassing of $^{129}Xe^*$ from the crust drove up the $^{129}Xe/^{132}Xe$ ratio. The spallation-derived xenon accumulated in today's atmosphere can be accounted for by a constant degassing rate of 0.034 % of the regolith budget of spallation produced xenon per Myr. If low level loss is permitted after collapse, a thicker atmosphere at the start of the model decreases the ability to produce spallation xenon. In order to accumulate sufficient spallation xenon in today's atmosphere, the initial atmosphere was no more than 4.9 times thicker than today's, with a corresponding loss rate no more than 0.043 % Myr^{-1}. For consistency with a $^{129}Xe^*$ degassing rather that decreases over time, the $^{129}Xe/^{132}Xe$ ratio recorded in Nakhla must have been trapped no more recently than 720 Myr ago.

In summary, combining the constraint on the $^{129}Xe/^{132}Xe$ ratio imposed by Nakhla with declining $^{129}Xe^*$ degassing rates, the model requires loss of xenon from the martian atmosphere over the last 3.7 Gyr (i.e., since collapse of an initial, thick atmosphere), and the present day budget is as little as 20 % of that at the start of this period.

Declaration of Competing Interest

The authors declare that they have no known competing financial interests or personal relationships that could have appeared to influence the work reported in this paper.

Data availability

Research data and supplementary information associated with this article can be access at doi: https://doi.org/10.48420/14229269

Acknowledgements

We thank University of Manchester undergraduate student Nicholas Jastrzebski for his help in collecting some of the data presented in this paper. We thank Drs. Lorraine Ruzié-Hamilton and John Cowpe for assistance with argon and halogen techniques, Dr. Tristan Lowe for assistance with CT scanning, and Dr Gavyn Rollinson (University of Exeter, Camborne School of Mines) is thanked for performing the QEMSCAN analysis. Work at the University of Manchester was supported by the Science and Technology Facilities Council (STFC), grants ST/J001643/1, ST/L002957/1, ST/M001253/1, and ST/R000751/1; KJ was also supported by a Royal Society University Research Fellowship (URF\R\201009) at the University of Manchester. PLC acknowledges funding support from UK Research and Innovation grant MR/S03465X/1. Parts of this work (HB) have been carried

out within the framework of the NCCR "PlanetS" supported by the Swiss NSF. We thank the NASA Solar System Workings program for support of LA-ICP-MS (MH). The National High Magnetic Field Laboratory is supported by the National Science Foundation through NSF/DMR-1644779 and the State of Florida. We are thankful for constructive reviews by Julia Cartwright and William Cassata and for editorial handling from Chris Herd.

Appendix A. Supplementary material

Supplementary material to this article can be found online at https://doi.org/10.1016/j.gca.2022.08.002.

References

Agee, C.B., Wilson, N.V., McCubbin, F.M., Ziegler, K., Polyak, V.J., Sharp, Z.D., Asmerom, Y., Nunn, M.H., Shaheen, R., Thiemens, M.H., Steele, A., Fogel, M.L., Bowden, R., Glamoclija, M., Zhang, Z., Elardo, S.M., 2013. Unique Meteorite from Early Amazonian Mars: Water-Rich Basaltic Breccia Northwest Africa 7034. Science 339, 780–785.

Ash, R.D., Knott, S.F., Turner, G., 1996. A 4-Gyr shock age for a martian meteorite and implications for the cratering history of Mars. Nature 380, 57–59.

Atreya, S.K., Trainer, M.G., Franz, H.B., Wong, M.H., Manning, H.L.K., Malespin, C.A., Mahaffy, P.R., Conrad, P.G., Brunner, A.E., Leshin, L.A., Jones, J.H., Webster, C.R., Owen, T.C., Pepin, R.O., Navarro-González, R., 2013. Primordial argon isotope fractionation in the atmosphere of Mars measured by the SAM instrument on Curiosity and implications for atmospheric loss. Geophys. Res. Lett. 40, 5605–5609.

Avice, G., Bekaert, D.V., Chennaoui Aoudjehane, H., Marty, B., 2018. Noble gases and nitrogen in Tissint reveal the composition of the Mars atmosphere. Geochem. Perspect. Lett. 6, 11–16.

Avice, G., Marty, B., 2020. Perspectives on Atmospheric Evolution from Noble Gas and Nitrogen Isotopes on Earth, Mars & Venus. Space Sci. Rev. 216, 36.

Basford, J.R., Dragon, J.C., Pepin, R.O., Coscio Jr., M.R., Murthy, V.R., 1973. Krypton and xenon in lunar fines. In: 4th Lunar and Planetary Science Conference Proceedings, pp. 1915–1955.

Beck, P., Pommerol, A., Zanda, B., Remusat, L., Lorand, J.P., Göpel, C., Hewins, R., Pont, S., Lewin, E., Quirico, E., Schmitt, B., Montes-Hernandez, G., Garenne, A., Bonal, L., Proux, O., Hazemann, J.L., Chevrier, V.F., 2015. A Noachian source region for the "Black Beauty" meteorite, and a source lithology for Mars surface hydrated dust? Earth Planet. Sci. Lett. 427, 104–111.

Becker, R.H., Pepin, R.O., 1984. The case for a martian origin of the shergottites: nitrogen and noble gases in EETA 79001. Earth Planet. Sci. Lett. 69, 225–242.

Bellucci, J.J., Nemchin, A.A., Whitehouse, M.J., Humayun, M., Hewins, R., Zanda, B., 2015. Pb-isotopic evidence for an early, enriched crust on Mars. Earth Planet. Sci. Lett. 410, 34–41.

Bellucci, J.J., Whitehouse, M.J., John, T., Nemchin, A.A., Snape, J.F., Bland, P.A., Benedix, G.K., 2017. Halogen and Cl isotopic systematics in Martian phosphates: Implications for the Cl cycle and surface halogen reservoirs on Mars. Earth Planet. Sci. Lett. 458, 192–202.

Best, M.G., 2003. Igneous and metamorphic petrology. Blackwell Publishers, Malden, MA.

Bogard, D.D., Clayton, R.N., Marti, K., Owen, T., Turner, G., 2001. Martian Volatiles: Isotopic Composition, Origin, and Evolution. Space Sci. Rev. 96, 425–458.

Bogard, D.D., Garrison, D.H., 1998. Relative abundances of argon, krypton, and xenon in the Martian atmosphere as measured in Martian meteorites. Geochim. Cosmochim. Acta 62, 1829–1835.

Bogard, D.D., Garrison, D.H., 1999. Argon-39-argon-40 "ages" and trapped argon in Martian shergottites, Chassigny, and Allan Hills 84001. Meteorit. Planet. Sci. 34, 451–473.

Bogard, D.D., Hörz, F., Johnson, P.H., 1986. Shock-implanted noble gases: An experimental study with implications for the origin of Martian gases in shergottite meteorites. J. Geophys. Res. Solid Earth 91, E99–E114.

Bogard, D.D., Johnson, P., 1983. Martian Gases in an Antarctic Meteorite? Science 221, 651–654.

Bottke W.F., Marchi S., Vokrouhlicky D., Robbins S., Hynek B. and Morbidelli A., 2015. New Insights into the Martian Late Heavy Bombardment, 46th Lunar and Planetary Science Conference. Lunar and Planetary Institute, Houston, Abstract #1484.

Bouvier, A., Blichert-Toft, J., Albarède, F., 2009. Martian meteorite chronology and the evolution of the interior of Mars. Earth Planet. Sci. Lett. 280, 285–295.

Bouvier, L.C., Costa, M.M., Connelly, J.N., Jensen, N.K., Wielandt, D., Storey, M., Nemchin, A.A., Whitehouse, M.J., Snape, J.F., Bellucci, J.J., Moynier, F., Agranier, A., Gueguen, B., Schönbächler, M., Bizzarro, M., 2018. Evidence for extremely rapid magma ocean crystallization and crust formation on Mars. Nature 558, 586–589.

Boynton, W.V., Ming, D.W., Kounaves, S.P., Young, S.M.M., Arvidson, R.E., Hecht, M. H., Hoffman, J., Niles, P.B., Hamara, D.K., Quinn, R.C., Smith, P.H., Sutter, B., Catling, D.C., Morris, R.V., 2009. Evidence for Calcium Carbonate at the Mars Phoenix Landing Site. Science 325, 61–64.

Brazzle, R.H., Pravdivtseva, O.V., Meshik, A.P., Hohenberg, C.M., 1999. Verification and interpretation of the I-Xe chronometer. Geochim. Cosmochim. Acta 63, 739–760.

Bultel, B., Viennet, J.-C., Poulet, F., Carter, J., Werner, S.C., 2019. Detection of Carbonates in Martian Weathering Profiles. J. Geophys. Res. Planets 124, 989–1007.

Busemann, H., Baur, H., Wieler, R., 2000. Primordial noble gases in "phase Q" in carbonaceous and ordinary chondrites studied by closed-system stepped etching. Meteorit. Planet. Sci. 35, 949–973.

Cannon, K.M., Mustard, J.F., Agee, C.B., 2015. Evidence for a widespread basaltic breccia component in the martian low-albedo regions from the reflectance spectrum of Northwest Africa 7034. Icarus 252, 150–153.

Carr, M.H., 2012. The fluvial history of Mars. Philos. Trans. R. Soc. A: Math., Phys. Eng. Sci. 370, 2193–2215.

Carr, M.H., Head, J.W., 2010. Geologic history of Mars. Earth Planet. Sci. Lett. 294, 185–203.

Cartwright, J.A., Gilmour, J.D., Burgess, R., 2013. Martian fluid and Martian weathering signatures identified in Nakhla, NWA 998 and MIL 03346 by halogen and noble gas analysis. Geochim. Cosmochim. Acta 105, 255–293.

Cartwright, J.A., Ott, U., Herrmann, S., Agee, C.B., 2014. Modern atmospheric signatures in 4.4 Ga Martian meteorite NWA 7034. Earth Planet. Sci. Lett. 400, 77–87.

Cassata, W.S., 2017. Meteorite constraints on Martian atmospheric loss and paleoclimate. Earth Planet. Sci. Lett. 479, 322–329.

Cassata, W.S., Shuster, D.L., Renne, P.R., Weiss, B.P., 2010. Evidence for shock heating and constraints on Martian surface temperatures revealed by $^{40}Ar/^{39}Ar$ thermochronometry of Martian meteorites. Geochim. Cosmochim. Acta 74, 6900–6920.

Cassata, W.S., Cohen, B.E., Mark, D.F., Trappitsch, R., Crow, C.A., Wimpenny, J., Lee, M.R., Smith, C.L., 2018. Chronology of martian breccia NWA 7034 and the formation of the martian crustal dichotomy. Science Advances 4, eaap8306.

Chechev, V.P., Sergeev, V.O., 2004. Estimating the Decay and Radiation Characteristics of ^{129}I. Meas Tech+ 47, 402–406. Translated from Izmeritel'naya Tekhnika 404, 458–461.

Clay, P.L., Burgess, R., Busemann, H., Ruzié-Hamilton, L., Joachim, B., Day, J.M.D., Ballentine, C.J., 2017. Halogens in chondritic meteorites and terrestrial accretion. Nature 551, 614.

Clay, P.L., Joy, K.H., O'Driscoll, B., Busemann, H., Ruzié-Hamilton, L., Burgess, R., Fellowes, J., Joachim-Mrosko, B., Pernet-Fisher, J., Strekopytov, S., Ballentine, C.J., 2020. Heavy halogen geochemistry of martian shergottite meteorites and implications for the halogen composition of the depleted shergottite mantle source. Am. Mineral. 105, 289–306.

Cohen B.E., Smith C.L., Lee M.R., Mark D.F., Almeida N., Cassata W.S., Hallis L., Smith A., Daly L., 2018. Northwest Africa 11522: A New Paired Stone of Martian Polymict Regolith Breccia Northwest Africa 7034, 49th Lunar and Planetary Science Conference. Lunar and Planetary Institute, Houston, Abstract #1900.

Conrad, P.G., Malespin, C.A., Franz, H.B., Pepin, R.O., Trainer, M.G., Schwenzer, S.P., Atreya, S.K., Freissinet, C., Jones, J.H., Manning, H., Owen, T., Pavlov, A.A., Wiens, R.C., Wong, M.H., Mahaffy, P.R., 2016. In situ measurement of atmospheric krypton and xenon on Mars with Mars Science Laboratory. Earth Planet. Sci. Lett. 454, 1–9.

Costa, M.M., Jensen, N.K., Bouvier, L.C., Connelly, J.N., Mikouchi, T., Horstwood, M.S. A., Suuronen, J.-P., Moynier, F., Deng, Z., Agranier, A., Martin, L.A.J., Johnson, T.E., Nemchin, A.A., Bizzarro, M., 2020. The internal structure and geodynamics of Mars inferred from a 4.2-Gyr zircon record. Proc. Natl. Acad. Sci. 117, 30973–30979.

Crow, C.A., Crowther, S.A., McKeegan, K.D., Turner, G., Busemann, H., Gilmour, J.D., 2020. Xenon systematics of individual lunar zircons, a new window on the history of the lunar surface. Geochim. Cosmochim. Acta 286, 103–118.

Crowther, S.A., Gilmour, J.D., 2013. The Genesis solar xenon composition and its relationship to planetary xenon signatures. Geochim. Cosmochim. Acta 123, 17–34.

Crowther, S.A., Mohapatra, R.K., Turner, G., Blagburn, D.J., Kehm, K., Gilmour, J.D., 2008. Characteristics and applications of RELAX, an ultrasensitive resonance ionization mass spectrometer for xenon. J. Anal. At. Spectrom. 23, 938–947.

Daly, L., Lee, M.R., Piazolo, S., Griffin, S., Bazargan, M., Campanale, F., Chung, P., Cohen, B.E., Pickersgill, A.E., Hallis, L.J., Trimby, P.W., Baumgartner, R., Forman, L. V., Benedix, G.K., 2019. Boom boom pow: Shock-facilitated aqueous alteration and evidence for two shock events in the Martian nakhlite meteorites. Science Advances 5, eaaw5549.

Dauphas, N., Pourmand, A., 2011. Hf–W–Th evidence for rapid growth of Mars and its status as a planetary embryo. Nature 473, 489–492.

Drake, M.J., Swindle, T.D., Owen, T., Musselwhite, D.S., 1994. Fractionated martian atmosphere in the nakhlites? Meteoritics 29, 854–859.

Dreibus, G., Wänke, H., 1987. Volatiles on Earth and Mars: A comparison. Icarus 71, 225–240.

Elkins-Tanton, L.T., 2008. Linked magma ocean solidification and atmospheric growth for Earth and Mars. Earth Planet. Sci. Lett. 271, 181–191.

Eugster, O., Michel, T., 1995. Common asteroid break-up events of eucrites, diogenites, and howardites and cosmic-ray production rates for noble gases in achondrites. Geochim. Cosmochim. Acta 59, 177–199.

Fanale, F.P., Cannon, W.A., Owen, T., 1978. Mars: Regolith adsorption and the relative concentrations of atmospheric rare gases. Geophys. Res. Lett. 5, 77–80.

Fanale, F.P., Postawko, S.E., Pollack, J.B., Carr, M.H., Pepin, R.O., 1992. Mars: epochal climate change and volatile history. In: Kieffer, H.H., Jakosky, B.M., Snyder, C.W., Matthews, M.S. (Eds.), Mars. The University of Arizona Press, pp. 1135–1179.

Garrison, D.H., Bogard, D.D., 1998. Isotopic composition of trapped and cosmogenic noble gases in several Martian meteorites. Meteorit. Planet. Sci. 33, 721–736.
Gellert, R., Rieder, R., Anderson, R.C., Brückner, J., Clark, B.C., Dreibus, G., Economou, T., Klingelhöfer, G., Lugmair, G.W., Ming, D.W., Squyres, S.W., d'Uston, C., Wänke, H., Yen, A., Zipfel, J., 2004. Chemistry of Rocks and Soils in Gusev Crater from the Alpha Particle X-ray Spectrometer. Science 305, 829–832.
Gellert, R., Rieder, R., Brückner, J., Clark, B.C., Dreibus, G., Klingelhöfer, G., Lugmair, G., Ming, D.W., Wänke, H., Yen, A., Zipfel, J., Squyres, S.W., 2006. Alpha Particle X-Ray Spectrometer (APXS): Results from Gusev crater and calibration report. J. Geophys. Res. Planets 111, E02S05.
Gierasch, P.J., Toon, O.B., 1973. Atmospheric Pressure Variation and the Climate of Mars. J. Atmos. Sci. 30, 1502–1508.
Gilmour, J.D., Lyon, I.C., Johnston, W.A., Turner, G., 1994. Relax - an Ultrasensitive, Resonance Ionization Mass-Spectrometer for Xenon. Rev. Sci. Instru. 65, 617–625.
Gilmour, J.D., Whitby, J.A., Turner, G., 1998. Xenon isotopes in irradiated ALH84001: Evidence for shock-induced trapping of ancient Martian atmosphere. Geochim. Cosmochim. Acta 62, 2555–2571.
Gilmour, J.D., Whitby, J.A., Turner, G., 2001. Disentangling xenon components in Nakhla: martian atmosphere, spallation and martian interior. Geochim. Cosmochim. Acta 65, 343–354.
Greeley, R., Spudis, P.D., 1981. Volcanism on Mars. Rev. Geophys. 19, 13–41.
Griffiths A.A., Burgess R., Joy K.H., Lowe T. and Withers P.J., 2014. Petrography and Composition of Martian Meteorite NorthWest Africa 8114, 77th Annual Meeting of the Meteoritical Society. Lunar and Planetary Institute, Houston, Abstract #5304.
Haberle, R.M., Tyler, D., McKay, C.P., Davis, W.L., 1994. A Model for the Evolution of CO2 on Mars. Icarus 109, 102–120.
Habermann M., Agee C., Spilde M., 2017. Multi-Layered Clast in Martian Breccia Northwest Africa 10922, 48th Lunar and Planetary Science Conference. Lunar and Planetary Institute, Houston, Abstract #2743.
Herzog, G.F., Caffee, M.W., 2014. 1.13 - Cosmic-Ray Exposure Ages of Meteorites. In: Holland, H.D., Turekian, K.K. (Eds.), Treatise on Geochemistry (Second Edition). Elsevier, Oxford, pp. 419–454.
Hewins, R.H., Zanda, B., Humayun, M., Nemchin, A., Lorand, J.-P., Pont, S., Deldicque, D., Bellucci, J.J., Beck, P., Leroux, H., Marinova, M., Remusat, L., Göpel, C., Lewin, E., Grange, M., Kennedy, A., Whitehouse, M.J., 2017. Regolith breccia Northwest Africa 7533: Mineralogy and petrology with implications for early Mars. Meteorit. Planet. Sci. 52, 89–124.
Hofmann B.A., Greber N.D., Greenwood R.C., 2014. New Data for NWA 7906, 7907 and 8171, Pairings of Mars Breccia NWA 7034, 77th Annual Meeting of the Meteoritical Society. Lunar and Planetary Institute, Houston, Abstract #5230.
Hohenberg, C.M., Marti, K., Podosek, F.A., Reedy, R.C., Shirck, J.R., 1978. Comparisons between observed and predicted cosmogenic noble gases in lunar samples. Lunar and Planetary Science Conference Proceedings 2, 2311–2344.
Hohenberg, C.M., Hudson, B., Kennedy, B.M., Podosek, F.A., 1981. Xenon spallation systematics in Angra dos Reis. Geochim. Cosmochim. Acta 45, 1909–1915.
Hu, S., Lin, Y., Zhang, J., Hao, J., Xing, W., Zhang, T., Yang, W., Changela, H., 2019. Ancient geologic events on Mars revealed by zircons and apatites from the Martian regolith breccia NWA 7034. Meteorit. Planet. Sci. 54, 850–879.
Hudson, G.B., Kennedy, B.M., Podosek, F.A., Hohenberg, C.M., 1989. The early solar system abundance of ^{244}Pu as inferred from the St. Severin chondrite. Lunar and Planetary Science Conference Proceedings 19, 547.
Humayun, M., Nemchin, A., Zanda, B., Hewins, R.H., Grange, M., Kennedy, A., Lorand, J.P., Gopel, C., Fieni, C., Pont, S., Deldicque, D., 2013. Origin and age of the earliest Martian crust from meteorite NWA 7533. Nature 503, 513–516.
Hunten, D.M., 1993. Atmospheric Evolution of the Terrestrial Planets. Science 259, 915–920.
Jagoutz E., Bowring S., Jotter R., Dreibus G., 2009. New U-Th-Pb Data on SNC Meteorite ALHA 84001, 40th Lunar and Planetary Science Conference. Lunar and Planetary Institute, Houston, Abstract #1662.
Jakosky, B.M., Jones, J.H., 1997. The history of Martian volatiles. Rev. Geophys. 35, 1–16.
Jakosky, B.M., Slipski, M., Benna, M., Mahaffy, P., Elrod, M., Yelle, R., Stone, S., Alsaeed, N., 2017. Mars' atmospheric history derived from upper-atmosphere measurements of ^{38}Ar/^{36}Ar. Science 355, 1408–1410.
Krietsch D., 2020. Alteration on asteroids, diversity of primordial volatiles and their carriers in carbonaceous chondrites, and martian shergottite sampling sites - studied by meteoritic noble gases. PhD Thesis. ETH Zurich.
Lammer, H., Chassefière, E., Karatekin, Ö., Morschhauser, A., Niles, P.B., Mousis, O., Odert, P., Möstl, U.V., Breuer, D., Dehant, V., Grott, M., Gröller, H., Hauber, E., Pham, L.B.S., 2013. Outgassing History and Escape of the Martian Atmosphere and Water Inventory. Space Sci. Rev. 174, 113–154.
Lapen, T.J., Righter, M., Brandon, A.D., Debaille, V., Beard, B.L., Shafer, J.T., Peslier, A. H., 2010. A Younger Age for ALH84001 and Its Geochemical Link to Shergottite Sources in Mars. Science 328, 347–351.
Lee, J.-Y., Marti, K., Severinghaus, J.P., Kawamura, K., Yoo, H.-S., Lee, J.B., Kim, J.S., 2006. A redetermination of the isotopic abundances of atmospheric Ar. Geochim. Cosmochim. Acta 70, 4507–4512.
Leya, I., Masarik, J., 2009. Cosmogenic nuclides in stony meteorites revisited. Meteorit. Planet. Sci. 44, 1061–1086.
Li, Y.-H., 2000. A compendium of geochemistry : from solar nebula to the human brain. Princeton University Press, Princeton, N.J..
Lindsay, F.N., Delaney, J.S., Göpel, C., Herzog, G.F., Hewins, R., Humayun, M., Nagao, K., Nyquist, L.E., Park, J., Setera, J.B., Shih, C.-Y., Swisher III, C.C., Zanda, B., Turrin, B.D., . ^{40}Ar/^{39}Ar ages of Northwest Africa 7034 and Northwest Africa 7533. Meteorit. Planet. Sci. 56, 515–545.
MacArthur, J.L., Bridges, J.C., Hicks, L.J., Burgess, R., Joy, K.H., Branney, M.J., Hansford, G.M., Baker, S.H., Schwenzer, S.P., Gurman, S.J., Stephen, N.R., Steer, E.D., Piercy, J.D., Ireland, T.R., 2019. Mineralogical constraints on the thermal history of martian regolith breccia Northwest Africa 8114. Geochim. Cosmochim. Acta 246, 267–298.
Mahaffy, P.R., Webster, C.R., Atreya, S.K., Franz, H., Wong, M., Conrad, P.G., Harpold, D., Jones, J.J., Leshin, L.A., Manning, H., Owen, T., Pepin, R.O., Squyres, S., Trainer, M., 2013. Abundance and Isotopic Composition of Gases in the Martian Atmosphere from the Curiosity Rover. Science 341, 263–266.
Mars Fact Sheet, https://nssdc.gsfc.nasa.gov/planetary/factsheet/marsfact.html, accessed 16/02/2021.
Marti K., Eberhardt P., Geiss J., 1966. Spallation, Fission, and Neutron Capture Anomalies in Meteoritic Krypton and Xenon, Zeitschrift für Naturforschung A, p. 398.
Marty, B., Altwegg, K., Balsiger, H., Bar-Nun, A., Bekaert, D.V., Berthelier, J.-J., Bieler, A., Briois, C., Calmonte, U., Combi, M., De Keyser, J., Fiethe, B., Fuselier, S.A., Gasc, S., Gombosi, T.I., Hansen, K.C., Hässig, M., Jäckel, A., Kopp, E., Korth, A., Le Roy, L., Mall, U., Mousis, O., Owen, T., Rème, H., Rubin, M., Sémon, T., Tzou, C.-Y., Waite, J.H., Wurz, P., 2017. Xenon isotopes in 67P/Churyumov-Gerasimenko show that comets contributed to Earth's atmosphere. Science 356, 1069–1072.
Mathew, K.J., Kim, J.S., Marti, K., 1998. Martian atmospheric and indigenous components of xenon and nitrogen in the Shergotty, Nakhla, and Chassigny group meteorites. Meteorit. Planet. Sci. 33, 655–664.
Mathew, K.J., Marti, K., 2001. Early evolution of Martian volatiles: Nitrogen and noble gas components in ALH84001 and Chassigny. J. Geophys. Res. Planets 106, 1401–1422.
Mathew, K.J., Marti, K., 2002. Martian atmospheric and interior volatiles in the meteorite Nakhla. Earth Planet. Sci. Lett. 199, 7–20.
McCubbin, F.M., Boyce, J.W., Novák-Szabó, T., Santos, A.R., Tartèse, R., Muttik, N., Domokos, G., Vazquez, J., Keller, L.P., Moser, D.E., Jerolmack, D.J., Shearer, C.K., Steele, A., Elardo, S.M., Rahman, Z., Anand, M., Delhaye, T., Agee, C.B., 2016. Geologic history of Martian regolith breccia Northwest Africa 7034: Evidence for hydrothermal activity and lithologic diversity in the Martian crust. J. Geophys. Res. Planets 121, 2120–2149.
McSween, H.Y., Treiman, A.H., 1998. Martian meteorites. Rev. Mineral Geochem., 36 6-01-06-54.
Mertens C.A.K., Riebe M.E.I. and Busemann H. (2021) Probability of cosmogenice Nucleide Production Rates, 52nd Lunar and Planetary Science Conference, Lunar and Planetary Institute, Houston, Abstract #2098.
Meshik, A., Hohenberg, C., Pravdivtseva, O., Burnett, D., 2014. Heavy noble gases in solar wind delivered by Genesis mission. Geochim. Cosmochim. Acta 127, 326–347.
Meteoritical Bulletin Database, http://www.lpi.usra.edu/meteor/metbull.php, accessed 11/10/2021.
Mohapatra R.K., Schwenzer S.P., Ott U., 2002. Krypton and Xenon in Martian Meteorites from Hot Deserts- The Low Temperature Component, 33rd Lunar and Planetary Science Conference. Lunar and Planetary Institute, Houston, Abstract #1532.
Mohapatra, R.K., Schwenzer, S.P., Herrmann, S., Murty, S.V.S., Ott, U., Gilmour, J.D., 2009. Noble gases and nitrogen in Martian meteorites Dar al Gani 476, Sayh al Uhaymir 005 and Lewis Cliff 88516: EFA and extra neon. Geochim. Cosmochim. Acta 73, 1505–1522.
Musselwhite, D.S., Drake, M.J., 2000. Early Outgassing of Mars: Implications from Experimentally Determined Solubility of Iodine in Silicate Magmas. Icarus 148, 160–175.
Muttik, N., McCubbin, F.M., Keller, L.P., Santos, A.R., McCutcheon, W.A., Provencio, P. P., Rahman, Z., Shearer, C.K., Boyce, J.W., Agee, C.B., 2014. Inventory of H2O in the ancient Martian regolith from Northwest Africa 7034: The important role of Fe oxides. Geophys. Res. Lett. 41, 8235–8244.
Nemchin, A.A., Humayun, M., Whitehouse, M.J., Hewins, R.H., Lorand, J.P., Kennedy, A., Grange, M., Zanda, B., Fieni, C., Deldicque, D., 2014. Record of the ancient martian hydrosphere and atmosphere preserved in zircon from a martian meteorite. Nat. Geosci. 7, 638.
Nyquist, L.E., Bogard, D.D., Shih, C.-Y., Greshake, A., Stöffler, D., Eugster, O., 2001. Ages and Geologic Histories of Martian Meteorites. Space Sci. Rev. 96, 105–164.
Nyquist, L.E., Shih, C.-Y., McCubbin, F.M., Santos, A.R., Shearer, C.K., Peng, Z.X., Burger, P.V., Agee, C.B., 2016. Rb-Sr and Sm-Nd isotopic and REE studies of igneous components in the bulk matrix domain of Martian breccia Northwest Africa 7034. Meteorit. Planet. Sci. 51, 483–498.
Ocker, K.D., Gilmour, J.D., 2004. Martian xenon components in Shergotty mineral separates: Locations, sources, and trapping mechanisms. Meteorit. Planet. Sci. 39, 1967–1981.
Ollila A.M., Newsom H.E., Wiens R.C., Maurice S., Sautter V., Mangold N., Clark B., Vaniman D., Blank J.G., Bridges J., Cousin A., Tokar R.L., Gasnault O., Forni O., Lasue J., Anderson R., Clegg S.M., Dyar M.D., Fabre C., Lanza N., Rosen-Gooding A. and Team M., 2014. Trace Element (Strontium, Barium, Rubidium and Lithium) Analyses by ChemCam for the First 360 Sols in Gale Crater, Mars, 45th Lunar and Planetary Science Conference. Lunar and Planetary Institute, Houston, Abstract #2490.
Ott, U., 1988. Noble gases in SNC meteorites: Shergotty, Nakhla. Chassigny. Geochim. Cosmochim. Acta 52, 1937–1948.
Owen, T., Biemann, K., Rushneck, D.R., Biller, J.E., Howarth, D.W., Lafleur, A.L., 1977. The composition of the atmosphere at the surface of Mars. J. Geophys. Res. 82, 4635–4639.

Ozima, M., Podosek, F.A., 2002. Noble Gas Geochemistry. Cambridge University Press.
Pepin, R.O., 1991. On the origin and early evolution of terrestrial planet atmospheres and meteoritic volatiles. Icarus 92, 2–79.
Pepin, R.O., 1994. Evolution of the Martian Atmosphere. Icarus 111, 289–304.
Pepin, R.O., 2000. On the isotopic composition of primordial xenon in terrestrial planet atmospheres. Space Sci. Rev. 92, 371–395.
Pepin, R.O., Becker, R.H., Rider, P.E., 1995. Xenon and Krypton Isotope in Extraterrestrial Regolith Soils and in the Solar-Wind. Geochim. Cosmochim. Acta 59, 4997–5022.
Pollack, J.B., Yung, Y.L., 1980. Origin and Evolution of Planetary Atmospheres. Annu. Rev. Earth. Pl. Sci. 8, 425–487.
Porcelli, D., Turekian, K.K., 2014. 6.16 - The History of Planetary Degassing as Recorded by Noble Gases. In: Holland, H.D., Turekian, K.K. (Eds.), Treatise on Geochemistry (Second Edition). Elsevier, Oxford, pp. 353–382.
Ragettli, R.A., Hebeda, E.H., Signer, P., Wieler, R., 1994. Uranium Xenon Chronology - Precise Determination of $\lambda_{sf}^{136}Y_{sf}$ for Spontaneous Fission of ^{238}U. Earth Planet. Sci. Lett. 128, 653–670.
Rao, M.N., Bogard, D.D., Nyquist, L.E., McKay, D.S., Masarik, J., 2002. Neutron Capture Isotopes in the Martian Regolith and Implications for Martian Atmospheric Noble Gases. Icarus 156, 352–372.
Riebe, M.E.I., Welten, K.C., Meier, M.M.M., Wieler, R., Barth, M.I.F., Ward, D., Laubenstein, M., Bischoff, A., Caffee, M.W., Nishiizumi, K., Busemann, H., 2017. Cosmic-ray exposure ages of six chondritic Almahata Sitta fragments. Meteorit. Planet. Sci. 52, 2353–2374.
Santos, A.R., Agee, C.B., McCubbin, F.M., Shearer, C.K., Burger, P.V., Tartèse, R., Anand, M., 2015. Petrology of igneous clasts in Northwest Africa 7034: Implications for the petrologic diversity of the martian crust. Geochim. Cosmochim. Acta 157, 56–85.
Sautter, V., Toplis, M.J., Beck, P., Mangold, N., Wiens, R., Pinet, P., Cousin, A., Maurice, S., LeDeit, L., Hewins, R., Gasnault, O., Quantin, C., Forni, O., Newsom, H., Meslin, P.-Y., Wray, J., Bridges, N., Payré, V., Rapin, W., Le Mouélic, S., 2016. Magmatic complexity on early Mars as seen through a combination of orbital, in-situ and meteorite data. Lithos 254–255, 36–52.
Scherer, P., Schultz, L., Loeken, T., 1994. Weathering and atmospheric noble gases in chondrites. Terra Scientific Publishing Company (TERRAPUB), Tokyo.
Scherf, M., Lammer, H., 2020. Did Mars Possess a Dense Atmosphere During the First ~400 Million Years? Space Sci. Rev. 217, 2.
Schwenzer S.P. and Ott U. (2006) Evaluating Kr- and Xe-Data in the Nakhlites and ALHA84001 - Does EFA Hide EFM?, 37th Lunar and Planetary Science Conference. Lunar and Planetary Institute, Houston, Abstract #1614.
Schwenzer, S.P., Herrmann, S., Ott, U., 2012. Noble gas adsorption with and without mechanical stress: Not Martian signatures but fractionated air. Meteorit. Planet. Sci. 47, 1049–1061.
Schwenzer, S.P., Greenwood, R.C., Kelley, S.P., Ott, U., Tindle, A.G., Haubold, R., Herrmann, S., Gibson, J.M., Anand, M., Hammond, S., Franchi, I.A., 2013. Quantifying noble gas contamination during terrestrial alteration in Martian meteorites from Antarctica. Meteorit. Planet. Sci. 48, 929–954.
Stephenson, P.C., Lin, Y., Leya, I., 2017. The noble gas concentrations of the Martian meteorites GRV 99027 and paired NWA 7906/NWA 7907. Meteorit. Planet. Sci. 52, 2505–2520.
Swindle, T.D., Caffee, M.W., Hohenberg, C.M., 1986. Xenon and other noble gases in shergottites. Geochim. Cosmochim. Acta 50, 1001–1015.
Swindle, T.D., Grier, J.A., Burkland, M.K., 1995. Noble gases in orthopyroxenite ALH84001: A different kind of martian meteorite with an atmospheric signature. Geochim. Cosmochim. Acta 59, 793–801.
Swindle, T., Jones, J., 1997. The xenon isotopic composition of the primordial Martian atmosphere: Contributions from solar and fission components. J. Geophys. Res. Planets 102, 1671–1678.
Taylor, G.J., 2013. The bulk composition of Mars. Geochemistry 73, 401–420.
Turner, G., Knott, S.F., Ash, R.D., Gilmour, J.D., 1997. Ar-Ar chronology of the Martian meteorite ALH84001: Evidence for the timing of the early bombardment of Mars. Geochim. Cosmochim. Acta 61, 3835–3850.
Turner, G., Harrison, T.M., Holland, G., Mojzsis, S.J., Gilmour, J., 2004. Extinct ^{244}Pu in ancient zircons. Science 306, 89–91.
Udry, A., Howarth, G.H., Herd, C.D.K., Day, J.M.D., Lapen, T.J., Filiberto, J., 2020. What Martian Meteorites Reveal About the Interior and Surface of Mars. J. Geophys. Res.: Planets 125. e2020JE006523.
Vogel, N., Heber, V.S., Baur, H., Burnett, D.S., Wieler, R., 2011. Argon, krypton, and xenon in the bulk solar wind as collected by the Genesis mission. Geochim. Cosmochim. Acta 75, 3057–3071.
Wieler, R., Baur, H., 1994. Krypton and xenon from the solar wind and solar energetic particles in two lunar ilmenites of different antiquity. Meteoritics 29, 570–580.
Wieler, R., Huber, L., Busemann, H., Seiler, S., Leya, I., Maden, C., Masarik, J., Meier, M. M.M., Nagao, K., Trappitsch, R., Irving, A.J., 2016. Noble gases in 18 Martian meteorites and angrite Northwest Africa 7812—Exposure ages, trapped gases, and a re-evaluation of the evidence for solar cosmic ray-produced neon in shergottites and other achondrites. Meteorit. Planet. Sci. 51, 407–428.
Wiens, R.C., Becker, R.H., Pepin, R.O., 1986. The case for a martian origin of the shergottites, II. Trapped and indigenous gas components in EETA 79001 glass. Earth Planet. Sci. Lett. 77, 149–158.
Wiens, R.C., Pepin, R.O., 1988. Laboratory shock emplacement of noble gases, nitrogen, and carbon dioxide into basalt, and implications for trapped gases in shergottite EETA 79001. Geochim. Cosmochim. Acta 52, 295–307.
Wittmann, A., Korotev, R.L., Jolliff, B.L., Irving, A.J., Moser, D.E., Barker, I., Rumble, D., 2015. Petrography and composition of Martian regolith breccia meteorite Northwest Africa 7475. Meteorit. Planet. Sci. 50, 326–352.
Yen, A.S., Gellert, R., Schröder, C., Morris, R.V., Bell Iii, J.F., Knudson, A.T., Clark, B.C., Ming, D.W., Crisp, J.A., Arvidson, R.E., Blaney, D., Brückner, J., Christensen, P.R., DesMarais, D.J., de Souza Jr, P.A., Economou, T.E., Ghosh, A., Hahn, B.C., Herkenhoff, K.E., Haskin, L.A., Hurowitz, J.A., Joliff, B.L., Johnson, J.R., Klingelhöfer, G., Madsen, M.B., McLennan, S.M., McSween, H.Y., Richter, L., Rieder, R., Rodionov, D., Soderblom, L., Squyres, S.W., Tosca, N.J., Wang, A., Wyatt, M., Zipfel, J., 2005. An integrated view of the chemistry and mineralogy of martian soils. Nature 436, 49.
Yin Q.-Z., McCubbin F.M., Zhou Q., Santos A.R., Targese R., Li X., Li Q., Liu Y., Tang G., Boyce J.W., Lin Y., Yang W., Zhang J., Hao J., Elardo S.M., Shearer C.K., Rowland D. J., Lerche M. and Agee C.B., 2014. An Earth-Like Beginning for Ancient Mars Indicated by Alkali-Rich Volcanism at 4.4 Ga, 45th Lunar and Planetary Science Conference. Lunar and Planetary Institute, Houston, Abstract #1320.
Zahnle, K.J., 1993. Xenological constraints on the impact erosion of the early Martian atmosphere. J. Geophys. Res. Planets 98, 10899–10913.
Zahnle, K.J., Gacesa, M., Catling, D.C., 2019. Strange messenger: A new history of hydrogen on Earth, as told by Xenon. Geochim. Cosmochim. Acta 244, 56–85.
Zahnle K., 1998. Origins of Atmospheres, Origins, p. 364.